Inorganica Chimica Acta 581 (2025) 122620

Contents lists available at ScienceDirect

Inorganica Chimica Acta

journal homepage: www.elsevier.com/locate/ica

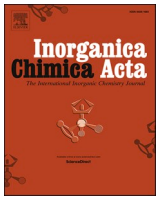

A new macrocyclic dansyl-cyclen fluorescent probe for the identification of mildly acidic intracellular compartments

Daniele Paderni [a,1], Daniele Lopez [b,1], Annarita Ciavarella [a], Mariele Montanari [b], Giovanna Panza [b], Maria Voccia [c], Mauro Formica [a], Barbara Canonico [b], Eleonora Macedi [a,*], Stefano Papa [b], Vieri Fusi [a,*]

[a] Department of Pure and Applied Sciences, University of Urbino Carlo Bo, 61029 Urbino, Italy
[b] Department of Biomolecular Sciences, University of Urbino Carlo Bo, 61029 Urbino, Italy
[c] Department of Materials Science, University of Milano Bicocca, 20126 Milan, Italy

ARTICLE INFO

Keywords:
Polyazamacrocycle
Dansyl
pH-probe
Fluorescence
Endo-lysosomes
Autophagy
Chloroquine

ABSTRACT

A new dansyl-based fluorescent probe containing the dimethylcyclen macrocycle scaffold (1,7-dimethyl-4,10-bis (dansyl)-1,4,7,10-tetraazacyclododecane, AJ2DAN) has been synthesized and fully characterized; it was designed based on a previous similar molecule (AJ2NBD), featuring two NBD (4-amino-7-nitrobenzo[1,2,5] oxadiazole) fluorophores in place of dansyl groups. Absorption and fluorescence emission spectra of AJ2DAN were recorded in both aqueous solution and organic solvents, always showing large Stokes shifts. In acidic solution the compound is very weakly fluorescent, while the emission increased by moving towards neutral pH. Moreover, a very high emission was detected in 1,4-dioxane, a solvent able to mimic the cell membrane polarity. The chemical response is reflected by the intracellular behaviour: by coupling AJ2DAN and LTDR labelling, it is possible to observe the lack of colocalization of "green" AJ2DAN^{positive} vesicles with LTDR^{positive} lysosomes, attesting a specificity for vesicular structures with mild acidic environment, such as autophagosomes and amphisomes. The autophagy inhibitor Chloroquine (CQ) has been used to prevent the fusion of autophagosomes with lysosomes and their consequent lysosomal degradation, thereby increasing the accumulation of autophagosomes: this drug enabled to set-up the protocol used in the present study. The new AJ2DAN molecule shows a high and pH-dependent quantum yield thus it lies in the field of fluorescent probes. Here, it has been demonstrated its possible use in the biological environment not only for cell imaging but also as pH-probe inside the biological compartments.

1. Introduction

Fluorescent probes have emerged as crucial tools in many research fields, ranging from fundamental research, to analytical and environmental analyses to biology and medicine [1–5]. Indeed, the employment of optical chemosensors offers advantages on instrumental methods and rests on high sensitivity and selectivity, simplicity, reliability, velocity and possibility to operate in real time conditions [6,7]. Many fluorescent probes have been studied for their ability to modulate their optical emission properties in the presence of target analytes or due to the different environment, as for example the polarity of the solvent [8–13]. More in particular, fluorescent chemosensors have been developed to detect intracellular species, such as metal cations, anions and other biomolecules [14], monitor physiological processes [15], and proved successful in drug sensing [2,16], immunofluorescence staining, live-cell imaging, drug delivery and fluorescence-guided surgery [17–23].

It must be considered that in most biological events the pH value plays a key role and requires a precise control, on pain of causing certain diseases [24,25]. Fluorescent probes represent a good strategy also for this task, in that they may monitor the pH value through the variation of the intensity or wavelength of the emission along with pH change [26,27]. Indeed, dansyl-based compounds have been widely studied as pH probes, due to the strong dependence of their fluorescence emission on the local environment [28–33].

Moreover, many dansyl-based molecules can bind and detect specific metal ions [34–37], and the metal complexes exhibited peculiar abilities

* Corresponding authors.
E-mail addresses: eleonora.macedi@uniurb.it (E. Macedi), vieri.fusi@uniurb.it (V. Fusi).
[1] These authors contributed equally to this work.

https://doi.org/10.1016/j.ica.2025.122620
Received 16 December 2024; Received in revised form 13 February 2025; Accepted 25 February 2025
Available online 5 March 2025
0020-1693/© 2025 The Authors. Published by Elsevier B.V. This is an open access article under the CC BY license (http://creativecommons.org/licenses/by/4.0/).

in the biological environment, such as production of DNA conformational switch [38], detection of base flipping of DNA [39], detection of hydrogen sulfide in hypoxia [40].

In this context, our research group has synthesized a new dansyl-based fluorescent probe built on the dimethylcyclen macrocycle scaffold (1,7-dimethyl-4,10-bis(dansyl)-1,4,7,10-tetraazacyclododecane, AJ2DAN, Fig. 1), to exploit the pH- and polarity-dependent emission of the fluorophore. The compound was designed based on a previous similar molecule (AJ2NBD), featuring two NBD (4-amino-7-nitrobenzo [1,2,5]oxadiazole) fluorophores in place of dansyl groups on the same polyazamacrocycle framework, that proved successful as a probe for vesicular trafficking [41,42].

The study of cellular organelles is indeed crucial to understand the mechanisms behind many biological processes. The employment of fluorescent probes is a convenient strategy also to this purpose, offering advantages over other techniques (electron microscope, high performance liquid chromatography, electrochemical methods), such as user friendly and fast analyses. Furthermore, fluorescent probes can be employed for real analytical single-cell analysis, demonstrating the power of flow cytometry. In particular, due to the acid-base properties of AJ2DAN, it has been tested as a pH-probe possibly useful to track specific vesicular processes involving acidic compartments.

Herein, we report the synthesis of the new AJ2DAN probe and the characterization of its acid-base properties in aqueous solution, as well as the robustness of the pH probe, *via* UV–Vis, fluorescence and NMR spectroscopic measurements. Besides the study of the fluorescence behaviour in aqueous solution as a function of pH, it was also investigated as a function of solvent polarity and in the presence of several metal ions. Moreover, structural features of the different protonated species of AJ2DAN present in water and 1,4-dioxane were studied by DFT calculations [43]. Finally, flow cytometry and confocal microscopy were used to study the possible employment of AJ2DAN as a dye for compartments involved in the endosomal/autophagic pathway and vesicular trafficking.

2. Experimental

2.1. Instruments and materials

All chemicals were purchased in the highest quality commercially available. The solvents were RP grade, unless otherwise indicated, and used without further purification. All reactions involving moisture-sensitive reagents were carried out under a nitrogen atmosphere using standard vacuum line techniques and glassware that was flame-dried before use.

The High-Resolution Mass Spectra were performed with an Orbitrap Exploris 240 Mass Spectrometer (Thermo Fisher Scientific, Milan, Italy) by direct infusion at 5 μL per minute and resolution set to 180 K FWHM. AGC target was set to standard mode and Max Injection time was set to 100 ms.

Picture depicted in Fig. 2d was taken with the digital camera of a common smartphone.

2.2. UV–Vis and fluorescence emission experiments

The spectrophotometric measurements were carried out at 298.1 K using a Varian Cary-100 spectrophotometer equipped with a temperature control unit. Uncorrected emission spectra were obtained with a Varian Cary Eclipse fluorescence spectrophotometer. Luminescence quantum yields were determined using quinine sulphate in a 0.5 mol dm^{-3} H_2SO_4 aqueous solution ($\Phi = 0.546$) as reference. In all cases, to ensure the complete solubilization of AJ2DAN, the compound was first dissolved in dimethyl sulfoxide (DMSO, $1.0{\cdot}10^{-3}$ mol dm^{-3}) then the solution was diluted with water or organic solvents (DMSO, acetonitrile, ethanol, 1,4-dioxane, $1.0{\cdot}10^{-5}$ mol dm^{-3}). In all cases, a $I = 1.0{\cdot}10^{-3}$ mol dm^{-3} NaCl (in water) or NMe_4Cl (in organic solvents) was used.

UV–Vis and fluorescence emission pH titrations and the reversibility measurement were performed by adding 0.1 mol dm^{-3} NaOH or HCl solutions to adjust the pH.

Screenings with alkaline, alkaline-earth, transition and rare earth metal ions were carried out by adding 1 equiv. of M^{n+} as their chloride or perchlorate salts to solutions of AJ2DAN ($1.0{\cdot}10^{-5}$ mol dm^{-3}) in water (pH 2 and 7, $M^{n+} = Li^+$, Na^+, K^+, Cs^+, Mg^{2+}, Ca^{2+}, Sr^{2+}, Ba^{2+}, Zn^{2+}, Cd^{2+}, Hg^{2+}, Pd^{2+}, Pt^{2+}, Cu^{2+}, Co^{2+}, La^{3+}, Nd^{3+}, Gd^{3+}) and 1,4-dioxane ($M^{n+} = Li^+$, Na^+, Mg^{2+}, Ca^{2+}, Zn^{2+}, Cd^{2+}, Cu^{2+}, Pd^{2+}, La^{3+}, Gd^{3+}).

2.3. NMR experiments

NMR spectra were recorded on a Bruker Avance Neo 600 spectrometer operating at 600.13 and 150.90 MHz for ^1H and ^{13}C, respectively, equipped with a BBFO *Z*-gradient SmartProbe (iProbe) and a variable temperature unit. The temperature of the NMR probe was calibrated using 1,2-ethandiol as calibration sample. Chemical shifts (δ scale) are reported in parts per million (ppm values) and are referenced to the residual solvent peak; coupling constants (*J* values) are given in hertz (Hz). ^1H—^1H and ^1H—^{13}C correlation experiments, performed to assign the signals (COSY, NOESY and HSQC), were conducted using standard Bruker pulse sequences. The 2D-NOESY experiments were conducted using a mixing time (*d*8) of 0.30 s.

The pH-metric NMR titration was carried out in D_2O-DMSO-d_6 2: 1 solvent at 318.0 K; the pH was adjusted by adding small amounts of KOD or DCl and measured directly into the NMR tube with a micro-electrode (pH = pD − 0.4). The tube was kept for 10 min at a temperature of 318.0 K before starting the acquisition of the spectrum.

The following abbreviations were adopted in reporting NMR data: singlet (s), doublet (d), triplet (t), quartet (q), quintet (quint), broad signal (bs), doublet of doublets (dd), doublet of doublet of doublets

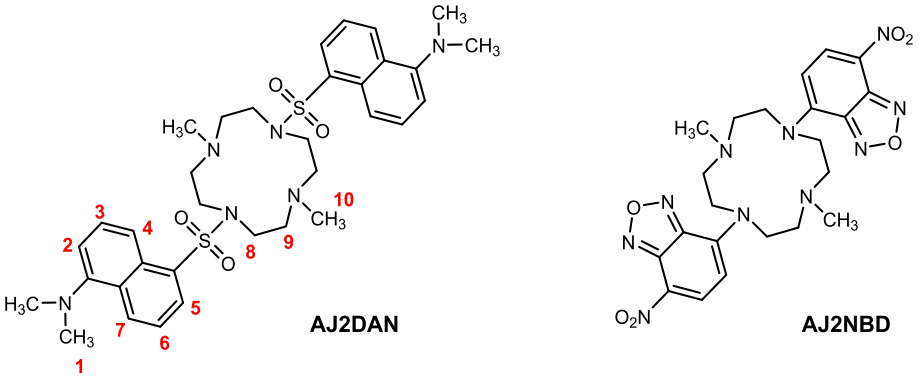

Fig. 1. The compound AJ2DAN studied in the present paper along with ^1H NMR labels and the previously studied compound AJ2NBD.

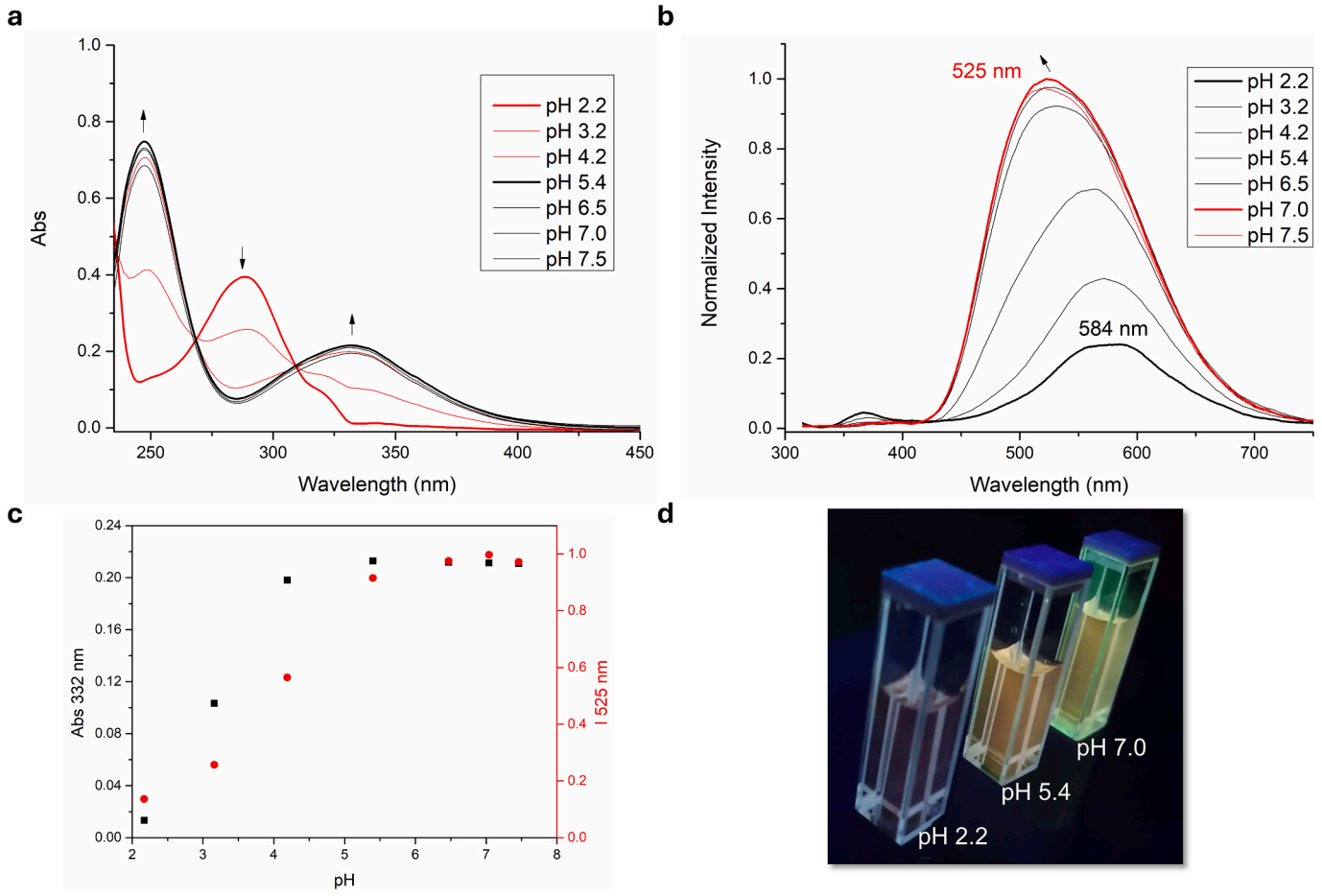

Fig. 2. a) Absorption and b) normalized fluorescence emission spectra of AJ2DAN in aqueous solution as a function of pH; c) trend of absorption at 332 nm (black squares) and of emission at 525 nm (red dots) as a function of pH; d) picture of aqueous solutions of AJ2DAN at different pH values under a 360 UV lamp. [AJ2DAN] = $3{\cdot}10^{-5}$ mol dm^{-3} (for absorption) or $1{\cdot}10^{-5}$ mol dm^{-3} (for emission) in H_2O + 1 % DMSO, λ_{ex} = 309 nm, $I = 1.0{\cdot}10^{-3}$ mol dm^{-3} NaCl. (For interpretation of the references to colour in this figure legend, the reader is referred to the web version of this article.)

(ddd), doublet of triplets (dt), doublet of quartets (dq), triplet of doublets (td), triplet of triplets (tt), quartet of triplets (qt) or multiplet (m).

Different operating concentrations suitable for NMR ($5{\cdot}10^{-3}$ mol dm^{-3}) and fluorescence ($1{\cdot}10^{-5}$ mol dm^{-3}) measurements were used, to cover the different sensibility of these techniques.

2.4. Synthesis

Compound **1** was prepared according to a previously reported procedure [44].

2.4.1. 1,7-dimethyl-4,10-bis(dansyl)-1,4,7,10-tetraazacyclododecane (AJ2DAN)

A solution of dansyl chloride (**2**, 500 mg, 1.85 mmol) in toluene (25 mL) was slowly added to a solution of **1** (185.3 mg, 0.93 mmol) and TEA (3.72 mmol, 518 μL) in toluene (25 mL), then the mixture was stirred at RT overnight. The TLC (silica gel, $CHCl_3$) confirmed the disappearance of the reactant **2**, then the mixture was filtered and the solvent was removed under vacuum, along with the excess of TEA. The solid residue was recrystallized from CH_2Cl_2, the yellow crystalline solid was filtered and dried (Y = 93 %).

^{1}H NMR (DMSO-d_6, 25 °C, ppm): δ = 8.58 (2H, d, J = 8.6 Hz), 8.36 (2H, d, J = 8.7 Hz), 8.08 (2H, d, J = 7.3 Hz), 7.69 (4H, m), 7.31 (2H, d, J = 7.5 Hz), 3.63 (8H, br s), 3.13 (8H, br s), 2.86 (12H, s), 2.74 (6H, s) (Fig. S1).

^{13}C NMR (DMSO-d_6, 25 °C, ppm): δ = 152.1, 133.3, 130.8, 130.2, 130.0, 129.1, 128.8, 124.2, 119.1, 116.0, 58.9, 46.9, 45.5, 40.7 (Fig. S2).

HRMS (in ACN): (positive mode, m/z) calculated 666.30, found 667.3086 for $[M + H]^+$, 334.1581 for $[M + 2H]^{2+}$ and 223.1078 for $[M + 3H]^{3+}$ (Fig. S3).

2.5. Computational details

All the DFT geometry optimizations of the conformers were performed at the GGA BP86 [45–47] level with the Gaussian16 package [48]. The electronic configuration of the systems and the reported free energies were described with the SVP [49] basis set for H, C, N, O, S, Li and Mg while for Zn and Cd the quasi relativistic sdd ECP [50] effective core potential was adopted, with the GD3BJ empirical dispersion [51]. All geometry optimizations were characterized as minimum through frequency calculations and were performed without symmetry constraints. Solvent effects were estimated with the PCM model using water and 1,4-dioxane as solvents [50]. To obtain the Gibbs energies thermal corrections were included from the gas-phase frequency calculations at the gas-phase level of theory (BP86/SVP/sdd ECP).

2.6. In vitro acute exposure of HT-29 and Caco-2 cells

HT-29 cell line is a human colorectal adenocarcinoma cell line and was cultured in RPMI 1640 Medium (Sigma- Aldrich, St Louis, MO, USA) supplemented with 10 % Heat-Inactivated Foetal Bovine Serum (FBS; Gibco; Thermo Fisher Scientific, Inc., Waltham, MA, USA), 1 % L-glutamine (Sigma-Aldrich, St Louis, MO, USA), and 1 % penicillin/

streptomycin (Sigma-Aldrich, St Louis, MO, USA) at 37 °C in humidified air with 5 % CO_2. Caco-2 cells were maintained in DMEM/F12 containing 10 % heat-inactivated foetal bovine serum (FBS), 2 mM glutamine, and 1 % antibiotics. Regarding experimental assays, HT-29 cells were seeded in 6-well plates at a density of $1.5{\cdot}10^5$ cells per well and exposed to different concentrations (50 μM and 5 μM) of chloroquine diphosphate (CQ 30 mM Invitrogen, Catalog n. L10382) and incubated for 4 h and 24 h. For the control, the cells were incubated with a medium only.

2.7. Flow cytometric (FC) analyses

Cytometric experiments were conducted using a FACSCanto II flow cytometer (BD Biosciences) equipped with an argon laser (488 nm, blue excitation), a helium-neon laser (633 nm, red excitation), and a solid-state diode laser (405 nm, violet excitation). Data acquisition and analysis were performed using FACSDiva™ software (BD Biosciences). At least 10,000 cellular events were acquired for each sample.

The new fluorescent probe for detecting vesicular trafficking AJ2DAN was used at the same concentration as the AJ2NBD dye [41] showing excellent results at this concentration. AJ2DAN was dissolved in DMSO at a concentration of 15 mM. Cells were incubated with 500 nM (final concentration) of AJ2DAN for 20 min at RT. To detect the vesicular trafficking in both HT-29 and Caco-2 cells, the cells were stained at t0 and analyzed at t0 and 36 h after the maintaining at low temperature (+4 °C).

Propidium Iodide (PI; Sigma-Aldrich, St Louis, MO, USA) staining assessed cell death. The cells were incubated for 10 min in the dark with PI 1 mg/mL. LysoTracker Deep Red (LTDR) dye (Thermo Fisher Scientific, USA) was used to mark and trace the lysosomes. LTDR 100 nM was used to mark the lysosomes, and after 30 min of incubation, the red lysosomal fluorescence was detected by flow cytometry [52]. To study the autophagic-like vacuole, the cells were incubated with 50 μM monodansylcadaverine MDC (Sigma-Aldrich, St Louis, MO, USA). Autophagy was assessed using the Autophagy Detection kit (ab139484; Abcam, Cambridge, UK) following the manufacturer's instructions [53,54]. The mean fluorescence (MFI) of the kit is a useful indicator of autophagic activity within a cell population. Following treatment, cells were incubated with 300 μL of the diluted green stain solution for 30 min at 37 °C in the dark for subsequent flow cytometry analysis.

2.8. Confocal microscopy (CM)

To evaluate the behaviour of the probe, the cells were grown on MatTek glass bottom chambers (MatTek Corporation) and stained with AJ2DAN (used at the same concentration of cytometric experiments). Images were taken with the 60× objective of the BC43 (Oxford Instruments Andor, United Kingdom). To evaluate the localization of AJ2DAN, we used co-labelling with LTDR in HT-29 CQ treated cells, which were observed by Nikon AXR confocal laser scanning microscopy with excitation light at 405 nm. The images were subjected to further processing and analysis using the ImageJ software (National Institutes of Health, Bethesda, MD, USA).

2.9. Statistical analyses

Data are shown as mean (or percentage, as indicated) ± standard deviation (SD) of at least two or three independent experiments. The means of the two groups were compared by using an unpaired *t*-test or one-way Analysis of Variance (ANOVA), followed by a post-hoc Bonferroni test. The *p*-values less than 0.05 were considered statistically significant. All statistical analyses were performed using GraphPad Prism 9.0.0 (GraphPad software, San Diego, CA, USA).

3. Results and discussion

3.1. Synthesis

Compound **1** (1,7-dimethyl-1,4,7,10-tetraazacyclododecane, dimethylcyclen) was obtained by following a previously reported procedure [44]. AJ2DAN was synthesized by treating **1** overnight with dansyl chloride (**2**) in the presence of TEA in toluene solution (Scheme 1). After removal of the solvent, the dry crude was recrystallized from CH_2Cl_2, to obtain AJ2DAN as a yellow crystalline solid in very good yield.

3.2. Acid-base properties in aqueous solution

The new AJ2DAN molecule is based on the versatile 1,4,7,10-tetraazacyclododecane macrocycle (cyclen), which is *trans* di-substituted with two methyl groups and functionalized with two dansyl fluorophore moieties. The compound is an analogue of our previously synthesized fluorescent probe AJ2NBD, containing two NBD fluorophores in place of the dansyl groups [41]. AJ2DAN contains two sulfonamides groups as well as two aliphatic and two aromatic amine functions, therefore possesses acid-base properties and different protonation forms can exist depending on the pH value. This feature, possibly coupled with a fluorescence emission that changes upon pH variation, is worthy of a thorough investigation, since the ability to act as a pH probe is a useful property both for environmental as well as biological applications. For this reason, the acid-base properties of AJ2DAN were investigated in aqueous solution by UV–Vis absorption, fluorescence and ^{1}H NMR spectroscopies in the pH range 2–8. Studies at higher pH values were prevented by the scarce solubility of the compound at the operating concentration.

The absorption spectra of AJ2DAN show the typical bands of the dansyl moiety (Fig. 2a). At acidic pH (pH = 2.2) a band with λ_{max} at 288 nm (ε = 13,150 cm^{-1} mol^{-1} dm^3) was visible, relative to the protonated dansyl -$N(CH_3)_2$ group (red thick band in Fig. 2a). As long as the pH was raised, such band decreased and two new bands with λ_{max} at 332 nm (ε = 7,050 cm^{-1} mol^{-1} dm^3) and 247 nm (ε = 24,800 cm^{-1} mol^{-1} dm^3) grew, suggesting the deprotonation of the dansyl dimethylamino group (black thick band in Fig. 2a). The protonated/deprotonated forms convert directly from one another, as indicated by the formation of two clear isosbestic points at 269 and 309 nm. By analysing the trend of the absorption at λ = 332 nm, it significantly changed between pH 2 and 5, reaching the maximum absorption at pH 5.4, then it remained unchanged (see black squares in Fig. 2c).

pH-dependent fluorescence emission spectra of AJ2DAN were recorded by exciting at both isosbestic points (Fig.s 2b and S4). In acidic solution the compound is very weakly fluorescent, while the emission increased by moving towards neutral pH. The quantum yield of fluorescence at pH 7.4 is $\Phi_{fl} = 0.07$, which is not so different from that of the dansyl acid ($\Phi_{fl} = 0.088$ at $1{\cdot}10^{-5}$ mol dm^{-3} [55]), suggesting that the emission of the dansyl group in AJ2DAN is not significantly quenched by a possible electron transfer from the amine functions of the macrocycle, contrarily to what observed for a mono-dansylated cyclen compound, that showed a $\Phi_{fl} = 0.0035$ at pH 7.4 and $1{\cdot}10^{-5}$ mol dm^{-3} [55]. This behaviour might be rationalized in terms of the presence in solution of a

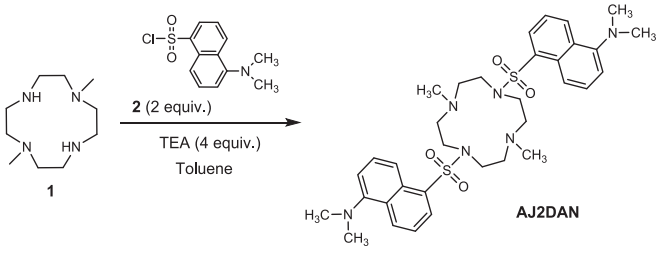

Scheme 1. Synthesis of the probe AJ2DAN.

monoprotonated macrocycle, where the two aliphatic amine functions share the proton *via* a hydrogen bond, and no nitrogen lone pairs are available for electron transfer (*vide infra*).

The observed fluorescence enhancement is ascribable to the deprotonation of the dansyl dimethylamino group (see Fig. 2c), that favours the charge transfer (CT) from the amine donor group to the sulfonamide acceptor group of the dansyl fluorophore. The PCT mechanism seems to be the only one at work in AJ2DAN: a Photoinduced Electron Transfer (PET) effect from the macrocycle nitrogen lone pairs to the excited state of the fluorophore can be indeed excluded, due to the observed increase of the fluorescence emission moving towards more alkaline pH values. A PET effect was instead observed for the NBD-analogue, whose fluorescence emission decreased along with the increase of pH [41].

When exciting at λ_{ex} = 269 nm, the spectrum obtained at pH 2.2 showed two bands (see Fig. S4, black thick line), which are ascribable to the dansyl -N(CH_3)$_2$ group in its protonated (band centred at 335 nm) and neutral (band centred at 554 nm) forms. The pH increase produced a drop of the intensity of the band at higher energy till its disappearance at pH > 5 (see inset of Fig. S4, black squares). On the contrary, the intensity of the band with λ_{max} at 554 nm increased by raising the pH, reaching a maximum around pH 7 (see Fig. S4, red thick line). The intensity stayed constant from now on (see inset in Fig. S4, red dots).

The excitation at the second isosbestic point (λ_{ex} = 309 nm) returned an analogous result in terms of emission enhancement along with pH increase up to neutral values. In this case, a blue-shift of the emission wavelength along with pH increase is also observed, with the band moving from 584 nm at pH 2.2 to 525 nm at pH 7.0 (see black and red thick lines in Fig. 2b). The wavelength change is clearly visible with the naked eye by observing aqueous solutions of AJ2DAN at pH around 2, 5 and 7 under a 360 nm UV lamp (Fig. 2d). The most acidic solution did not show any emission, while those at pH 5 and 7 exhibited yellow-orange and yellow emissions, respectively.

The acid-base properties of AJ2DAN were also studied by performing a ^{1}H NMR pH titration in mixed water-DMSO (2:1 *v*/v) solution between pH 2.2 and pH 7.4 (Fig. 3), due to the low solubility in pure water at such concentrations. More alkaline pH values could not be explored due to the scarce solubility of AJ2DAN also in this condition. By analysing the spectra at growing pH values, it can be clearly observed that some resonances are much more affected than others by the change of the pH. As far as the aliphatic resonances are concerned, the signal of the -N(CH_3)$_2$ methyl groups of the dansyl moiety (H1) significantly upfield shifted, moving from pH 2.2 to pH 7.4. The resonances attributed to the -CH_2 groups of the macrocycle also shifted upfield, even if to a lesser extent compared to the previous one. As for the aromatic resonances, mainly two of them shifted upfield (H7 and H2), the remaining signals shifted also upfield, even if to a lesser extent (Fig. S5). This behaviour may be rationalized in terms of the deprotonation of both the macrocycle and dansyl amine functions with the consequent increased electronic density. Moreover, the shifts are marked up to pH 4.5, while the spectrum recorded at higher pH (7.4) showed very similar chemical shifts to the previous ones for all peaks. This agrees well with the pK_a values of the involved groups (pK_a -N(CH_3)$_2$ dansyl group ≈ 4 [28,56,57]; pK_{a1} and pK_{a2} of macrocycle amine functions in AJ2NBD (4.2 and 9.7 [41]) and a similar mono-dansylated compound (3.5 and 9.7 [55]).

By merging the absorption, emission and NMR data, it can be hypothesized that at acidic pH values (≈ 2) AJ2DAN is present as both protonated $H_4\mathbf{L}^{4+}$ and $H_3\mathbf{L}^{3+}$ species, while at pH values ≈ 5 AJ2DAN lost both a macrocycle proton as well as the dansyl amine protons to form the $H\mathbf{L}^{+}$ species . Above pH 5 it can be thus suggested that the compound features only one proton in the macrocycle cage ($H\mathbf{L}^{+}$ form), that is probably shared between the two aliphatic amine functions *via* a hydrogen bond (Fig. S6). The neutral species of AJ2DAN, that could in principle be obtained by removing the remaining macrocycle proton, cannot form in the present experimental conditions, since a pH as high as ≈ 10 is required. It can be quite safely claimed that, due to the basicity of the compound, the probe is present in aqueous solution at physiological pH as monoprotonated $H\mathbf{L}^{+}$ form.

3.3. Evaluation of the robustness of the probe in aqueous solution

In view of a possible practical application as a fluorescent pH probe, it is crucial to evaluate the robustness of the probe, in terms of stability in solution, reversibility of emission with pH and interference from other ions in solution.

The stability of AJ2DAN was investigated in aqueous solution at pH 7.4 by both UV–Vis and ^{1}H NMR spectroscopies. Measurements showed a high stability of the compound, up to at least two weeks (Fig. S7). In the case of UV–Vis experiments, a buffer HEPES solution was used, while for NMR measurements AJ2DAN was dissolved in a D_2O: DMSO-d_6 2: 1 mixture to overcome solubility issues at the higher concentration used

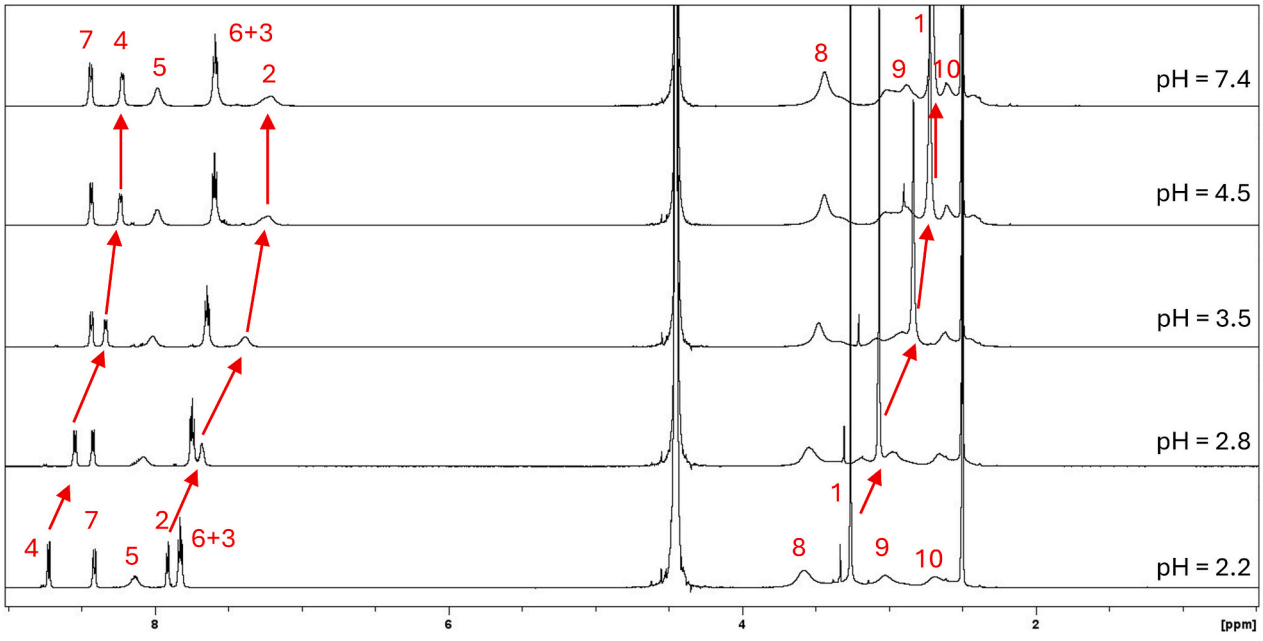

Fig. 3. ^{1}H NMR spectra of AJ2DAN in D_2O: DMSO-d_6 2: 1 at 318 K as a function of pH. [AJ2DAN] = 5·10^{-3} mol dm^{-3}.

for this analysis. The pH of the solution was checked during the whole period of the analysis.

The reversibility of the fluorescence emission of the system with pH was validated *via* modulation of pH values of a solution of AJ2DAN repeatedly between 2 and 7, and then recording the fluorescence intensity changes (Fig. 4). The intensity significantly decreased at pH 2, but the emission is recovered at pH 7, suggesting a good reversible response to pH change. Moreover, the reversible cycle can be repeated several times (up to at least 5 times) with negligible intensity change.

To assess whether common metal ions could interfere with the pH sensitivity of the probe, which would prevent a practical use in solution, several cations have been examined through fluorescence emission measurements. Alkali, alkaline-hearth, transition and rare earth metal ions have been tested to this purpose, and none of them displayed significant interference with fluorescence emission intensity and wavelength (Fig. 5). This behaviour highlights the scarce coordination properties of AJ2DAN towards such metal ions in aqueous solution at the pH values investigated. This is probably due both to the presence of an acidic proton within the macrocyclic ring, that is in competition with the binding of the metal ion by the two amine functions, and the unfavourable position of these latter to metal coordination. The similar compound mono-dansyl cyclen can instead bind the Zn^{2+} and Cu^{2+} cations, by virtue of the three amine functions of the macrocycle [38–40,55]. Given the stability, reversibility and insensitivity to other cations, AJ2DAN can be considered a promising probe for pH change detection in aqueous solutions.

3.4. DFT calculations in water

In order to gain insight into the structural features of the protonated forms of the AJ2DAN compound, a theoretical study at the DFT level [43] was undertaken, by adopting the BP86/SVP level of theory for the optimizations in the gas phase, and the B3LYP/TZVP level of theory in water as solvent, using a PCM model. Different conformations (open, closed, partially open) have been chosen and optimized for each protonation form (see Fig.s S6 and S8). An analysis of the optimized geometries shows for the $H_4\mathbf{L}^{4+}$ species a convergence always towards an open structure, irrespective of the starting geometry. In the case of the $H_3\mathbf{L}^{3+}$ species, besides the preferred open structure, a partially open conformation has been observed . The preference for the open structure shown by the highest charged species $H_4\mathbf{L}^{4+}$ and $H_3\mathbf{L}^{3+}$, with both dansyl side arms located on the same side with respect to the dimethylcyclen macrocycle and lying almost parallel to it, agrees with the dansyl

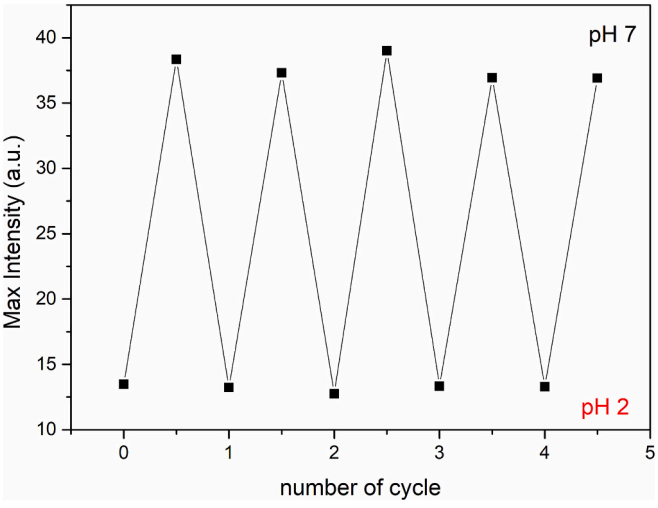

Fig. 4. Reversible changes of fluorescence intensity at 584 nm (pH 2) and 525 nm (pH 7) of AJ2DAN in H_2O + 1 % DMSO solution. [AJ2DAN] = $1{\cdot}10^{-5}$ mol dm^{-3}, λ_{ex} = 309 nm, $I = 1.0{\cdot}10^{-3}$ mol dm^{-3} NaCl.

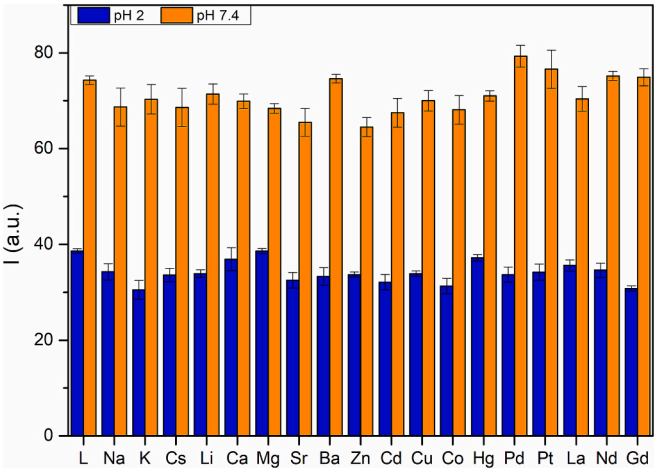

Fig. 5. Fluorescence emission changes of aqueous solutions of AJ2DAN at pH 2 and 7 before and after the addition of various metal ions (1 equiv). [AJ2DAN] = $1{\cdot}10^{-5}$ mol dm^{-3}, λ_{ex} = 288 nm (pH 2) and 330 nm (pH 7), $I = 1.0{\cdot}10^{-3}$ mol dm^{-3} NaCl.

groups being protonated, which induces an electrostatic repulsion that forces them to stay apart from each other. The presence of a hydrogen bond between the opposite aliphatic amine functions in $H_3\mathbf{L}^{3+}$ confers the macrocycle a more elongated rectangular shape (*trans* N—N distances 2.8 and 5.2 Å) than in $H_4\mathbf{L}^{4+}$ (*trans* N—N distances 4.8 and 3.8 Å). As a result, the SO_2 groups in $H_3\mathbf{L}^{3+}$ are more displaced (7.0 Å) than in $H_4\mathbf{L}^{4+}$ (4.3 Å). On the contrary, the monoprotonated $H\mathbf{L}^{+}$ species exhibited an energetic preference for a closed conformation, with the dansyl side arms almost reaching for each other above the macrocycle cavity, that appears rectangular as in $H_3\mathbf{L}^{3+}$ with very similar *trans* N—N distances (2.8 and 5.2 Å) and a larger displacement of the SO_2 groups (8.3 Å). The open and partially open structures lie 2.4 and 4.3 kcal/mol higher that the closed one (Fig. S8).

3.5. Analyses in organic solvents

Due to a strong polarity-dependence of the fluorescence emission of the dansyl group, the photophysical properties of AJ2DAN were also studied in various types of solvents with different polarity. The normalized absorption and emission spectra of AJ2DAN in ACN, DMSO, EtOH and dioxane were compared with those in water (HEPES pH 7.4)

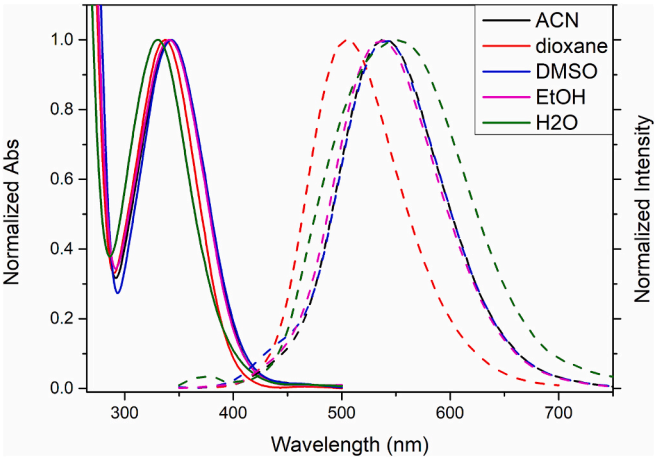

Fig. 6. Normalized absorption (solid lines) and fluorescence emission (dashed lines) spectra of AJ2DAN in different solvents. [AJ2DAN] = $1{\cdot}10^{-5}$ mol dm^{-3}, λ_{ex} = 345 nm for DMSO, EtOH, ACN, 335 nm for dioxane, 309 nm for water, $I = 1.0{\cdot}10^{-3}$ mol dm^{-3} NaCl (in water) or NMe_4Cl (organic solvents).

in Fig. 6. Absorption peaks are quite similar in all solvents, that in water shows the highest blue-shift (Table 1). Fluorescence emission peaks are similar for DMSO, EtOH and ACN, both in wavelength and intensity, while that in water gave the largest peak, centred at 525 nm, and the lowest intensity. Emission in dioxane exhibited the highest blue-shift, due to the lower polarity of the solvent compared to the others. The emission intensity in all organic solvents is higher than in water, with the largest fluorescence quantum yield observed for dioxane ($\Phi_{fl} = 1.0$). AJ2DAN exhibits very high Stokes shifts in all solvents, the highest being in water (11,164 cm^{-1}, corresponding to 194 nm) (Table 1). This latter finding is remarkable if considering that commercial dyes such as LysoTracker show much smaller Stokes shift (20 nm). A large Stokes shift is a quite favorable property, indeed AJ2DAN would prevent unwanted events such as self-reabsorption and inner filter effects.

The emission behaviour in dioxane has been studied due to the similarity between the dielectric constant of the solvent (Table 1) and cell membranes. Therefore, dioxane can mimic the lipid compartment and would allow to discover a possible membrane localization.

The photophysical properties of AJ2DAN in dioxane were therefore further explored. In particular the binding properties in such solvent were investigated towards several alkali, alkaline-earth, transition and rare earth metal cations, to verify whether the fluorescence properties were influenced by the presence of such guests, contrarily to what observed in aqueous solution (Fig. 7). Upon the addition of 1 equiv. of Zn^{2+} and Cd^{2+}, the dansyl band (338 nm) exhibited a small red shift (+ 3 nm), while no significant changes were detected in the presence of rare earth, alkali and alkaline-earth ions (Fig. S9).

All the tested metal ions induced a change in the emission spectrum of AJ2DAN, the most relevant results concerning the transition metal ions, that induced a partial quenching of the fluorescence emission (max −30 % for Cu^{2+}) and a red shift (+ 13 nm for Zn^{2+} and Cd^{2+}, + 15 nm for Cu^{2+} and + 3 nm for Pd^{2+}) (Fig.s S10 and 7). Small red shifts are also observed for Ca^{2+} (+ 3 nm), Mg^{2+} (+ 5 nm), Gd^{3+} (+ 2 nm) and La^{3+} (+ 3 nm).

Since the metal ions are added to the probe dissolved in dioxane as aqueous solutions, a possible interference of water on the fluorescence emission of AJ2DAN upon the addition of the guests was worthy of attention. For this reason, to a solution of AJ2DAN in dioxane, already containing 1.5 % of water, more water has been added to the solution up to further 0.8 % (25 μL, see experimental part for more details). The maximum quenching observed was of 5 %, much lower than those induced by the interaction with the guests. Therefore, it can be quite safely inferred that the variations observed are due to the metal ions.

Due to the proposed PCT fluorescence mechanism, the observed red shifts are supposed to depend by the interaction of the metal cations with the acceptor group of the dansyl fluorophore. In other words, the cations are more likely coordinated by the donor atoms of the macrocycle, included, at least partially, those belonging to sulphonamide groups.

3.6. DFT calculations in 1,4-dioxane

Due to the interesting fluorescence properties shown by AJ2DAN in dioxane, a theoretical study at the DFT level of theory was undertaken on the neutral form of the compound (**L**) using 1,4-dioxane as solvent, similarly to the previous study in water (Fig. S11). An analysis of the optimized geometries shows that a partially open conformation is the preferred one among the tested geometries (open, closed, partially open). The most stable conformation is probably driven by the formation of a weak hydrogen bond between an aromatic hydrogen atom of the dansyl group and the nitrogen atom of an aliphatic amine of the macrocycle (C···N 3.24 Å, H···N 2.22 Å, C-H···N 153.1°).

The optimized geometries were used as the starting point for the optimization of complexes with some of the tested metal cations, to gain insight into the structural features of the compounds. Moreover, the bond dissociation energies (BDEs) have also been investigated for the $[M(\mathbf{L})]^{n+} \rightarrow [M]^{n+} + (\mathbf{L})$ process (**L** = neutral AJ2DAN) [58–61], to compare the relative stability of the complexes with different metal ions in dioxane as solvent. The considered reactions and the relative calculated energies are reported in Fig. S12. From those data it can be inferred that *i)* the formation of all $[M(\mathbf{L})]^{n+}$ complexes is possible, being all BDEs >> 0 kcal/mol and *ii)* the zinc and the lithium complexes showed, respectively, the highest and the lowest BDE values, representative of the highest and lowest stability within the series of $[M(\mathbf{L})]^{n+}$, respectively. By looking at the calculated structures of the complexes, all of them exhibited a penta-coordination, with the metal ion bonded to the four nitrogen atoms of the macrocycle and to one oxygen atom of a SO_2 group (see the $[Li(\mathbf{L})]^{+}$ complex in Fig. S12 as evidence of all structures, that appeared all similar to the representative one). This is in line with the hypothesis that the red shift observed in the fluorescence emission upon addition of metal ions is due to the interaction of the guests with the acceptor group of the dansyl moiety (*vide supra*).

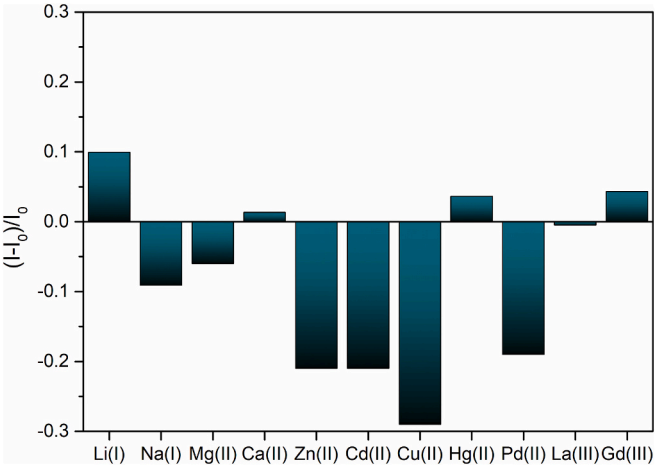

Fig. 7. Fluorescence emission changes of solutions of AJ2DAN in dioxane after the addition of various metal ions (1 equiv). [AJ2DAN] = $1{\cdot}10^{-5}$ mol dm^{-3}, λ_{ex} = 335 nm, $I = 1.0{\cdot}10^{-3}$ mol dm^{-3} NMe_4Cl.

Table 1
Spectrophotometric parameters of AJ2DAN in different solvents (λ_{ex} = 345 nm for DMSO, EtOH, ACN, 335 nm for dioxane, 309 nm for water); ε_r: dielectric constant of the solvent; λ_{abs} and λ_{em}: maxima of the absorption and emission wavelengths; Δ_{ss}: Stokes shift in cm^{-1}.

Solvent	ε_r	λ_{abs} (nm)	λ_{em} (nm)	Δ_{ss} (cm^{-1})
Water	80.1	331	525	11,164
Dimethyl sulfoxide (DMSO)	46.7	343	540	10,636
Acetonitrile (ACN)	36.7	341	537	10,704
Ethanol (EtOH)	24.3	341	536	10,669
Dioxane	2.20	338	505	9,784

3.7. Biological studies

3.7.1. AJ2DAN staining on two tumor intestinal cell lines

HT-29 and Caco-2 cells were chosen for the present study, since they both represent a model of Colorectal cancer (CRC). CRC is the third most common cancer and the cause of cancer related-death in both men and women worldwide [62,63]. One of the major reasons for poor prognosis and therapy failure in CRC patients is multidrug resistance (MDR), a phenomenon in which cancer cells develop cross-resistance to anticancer drugs of different structures and pharmacological mechanisms of action [64]. Different researchers reported that dysregulation in *endo*-lysosomal compartments is involved in mediating MDR through multiple mechanisms, such as alterations in endosomes, lysosomes and autophagosomes, that traffic and biodegrade the molecular cargo [65]. For these reasons, HT-29 and Caco-2 intestinal cell lines were firstly

chosen to test the labelling features of AJ2DAN.

AJ2DAN was added to HT-29 and Caco-2 cells to set staining parameters and cell conditions. Fluorescence was collected at 490–500 nm, whereas the laser line was tuned at 405 nm. Based on the above chemical evaluations, it must be pointed out that: *i)* excitation at 405 nm corresponds to a very low absorption in solution (Fig. 6), noteworthy the fluorescence intensity is anyway enough for cell imaging; *ii)* the emission wavelength in the 490–500 nm range agrees better with the observed emission in dioxane than in water solution (Table 1), which suggests a possible membrane localization of AJ2DAN.

Also, based on the above chemical evaluations (*vide supra*), the choice of the described channels allowed us to delineate a panel with additional fluorochromes and, in particular, to draw the histograms of the sole AJ2DAN labelling (Fig. 8). The tumor intestinal cell line HT-29 highlights a good brightness for the fluorochrome, underlined by the high fold of increase of the specific fluorescence concerning unstained samples (Fig. 8A,B). Similarly, Caco-2 cells showed high fluorescence values (Fig. 8C,D), although mildly reduced, as also demonstrated by fluorescence raw data for both cell lines (Fig. S13). Furthermore, confocal analyses of stained HT-29 cells (Fig. 8Ea,b) addressed the specific localization of intracellular structures pointed out by AJ2DAN staining, that appear as green dots, mainly perinuclear, and are exhibited by all cells although with different brightness. Finally, after 30 min of AJ2DAN addition to the cells, no process of cell death induction was observed.

3.7.2. *AJ2DAN fluorescence retention in both analyzed cell lines*

To evaluate the degree of cell retention of AJ2DAN fluorescence during time, cells were analyzed by Flow Cytometry after 36 h storage at 4 °C of labelled and unlabelled tubes. In agreement with other protocols of cell storage, Hunt et al. [66] shown that adherent cell cultures of mammalian cells can be stopped for short periods (days to weeks) in standard media at temperatures between 4 °C and 24 °C. In cultured mammalian cells, after a quiescence period, viable cells continued to divide and were used for routine applications. Histograms report a well detectable fluorescence (Fig. 9A-D), not significantly reduced with respect to the same fluorescence values collected on fresh cells, after 20 min of incubation with AJ2DAN (Fig. 9E,F). The same scenario is shown by both HT-29 and Caco-2 cells, suggesting that the staining properties of the dye and its retention are independent of cell type.

3.7.3. *Cytotoxicity study of AJ2DAN*

During the 36 h of storage at 4 °C, besides the fluorescence retention, also the possible toxicity of the dye was evaluated through the combination of AJ2DAN with Propidium Iodide (PI), a fluorochrome largely employed in biological studies to evaluate cell death. Data in Fig. 10 demonstrated that the combination of the two dyes is readily detectable in a bi-parametric dot plot, allowing for a double colour analysis and identification of dead cells (red events) and still viable cells (green events; HT-29 in Fig. 10A, Caco-2 in Fig. 10B). Interestingly, 36 h of cell exposure to the dye did not induce any significant additional cell death process, except those caused by a long time of low-temperature exposition; indeed the same percentages of dead cells are detected in both samples, with and without AJ2DAN, as demonstrated by statistic histograms related to both HT29 (Fig. 10C) and Caco-2 cells (Fig. 10D). Mean Fluorescence Intensity (MFI) values collected for the same samples depict a specific AJ2DAN fluorescence decrease for dead cells, highlighted by the red histograms in Fig. 10E,F.

All the findings suggest that AJ2DAN specifically labels membrane organelles, vesicular-like, with a perinuclear distribution. Indeed when cells lose their viability, AJ2DAN fluorescence drops, suggesting that these vesicles/vacuoles lose their function and/or structure.

3.7.4. *Establishing the nature of intracellular structures traced by AJ2DAN: The endo-lysosome and autophagosome network*

To better define the puncta perinuclear distribution of AJ2DAN fluorescence, co-staining by AJ2DAN and LTDR was applied. As previously shown (Fig. 8E), confocal analyses were exclusively conducted on HT-29 cells since they exhibit a higher proliferation rate, a well-defined lysosomal network and good staining by AJ2DAN. Indeed, besides control samples, chloroquine-treated samples have been analyzed (Fig. 11A,B,C). Chloroquine (CQ) is an anti-malarial drug [67] that has

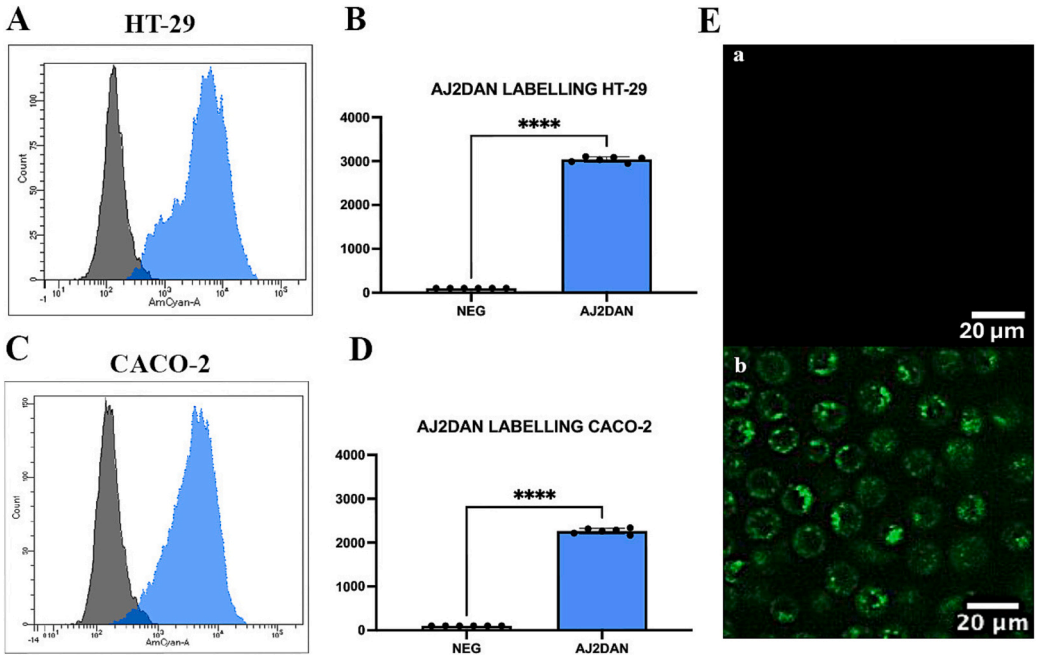

Fig. 8. A HT-29 cells: FC histograms at t0 (unlabelled in grey and AJ2DAN-labelled in blue); B Statistical histogram: MFI ratio from AJ2DAN-labelled and unlabelled HT-29 cells and at t0; C Caco-2 cells: FC histograms at t0; D Statistical histogram: MFI ratio from AJ2DAN-labelled and unlabelled Caco-2 cells and at t0; E Confocal images of HT-29 cells: unlabelled (Ea) and AJ2DAN-labelled (Eb). Unpaired *t*-test revealed: **** = $p < 0.0001$. (For interpretation of the references to colour in this figure legend, the reader is referred to the web version of this article.)

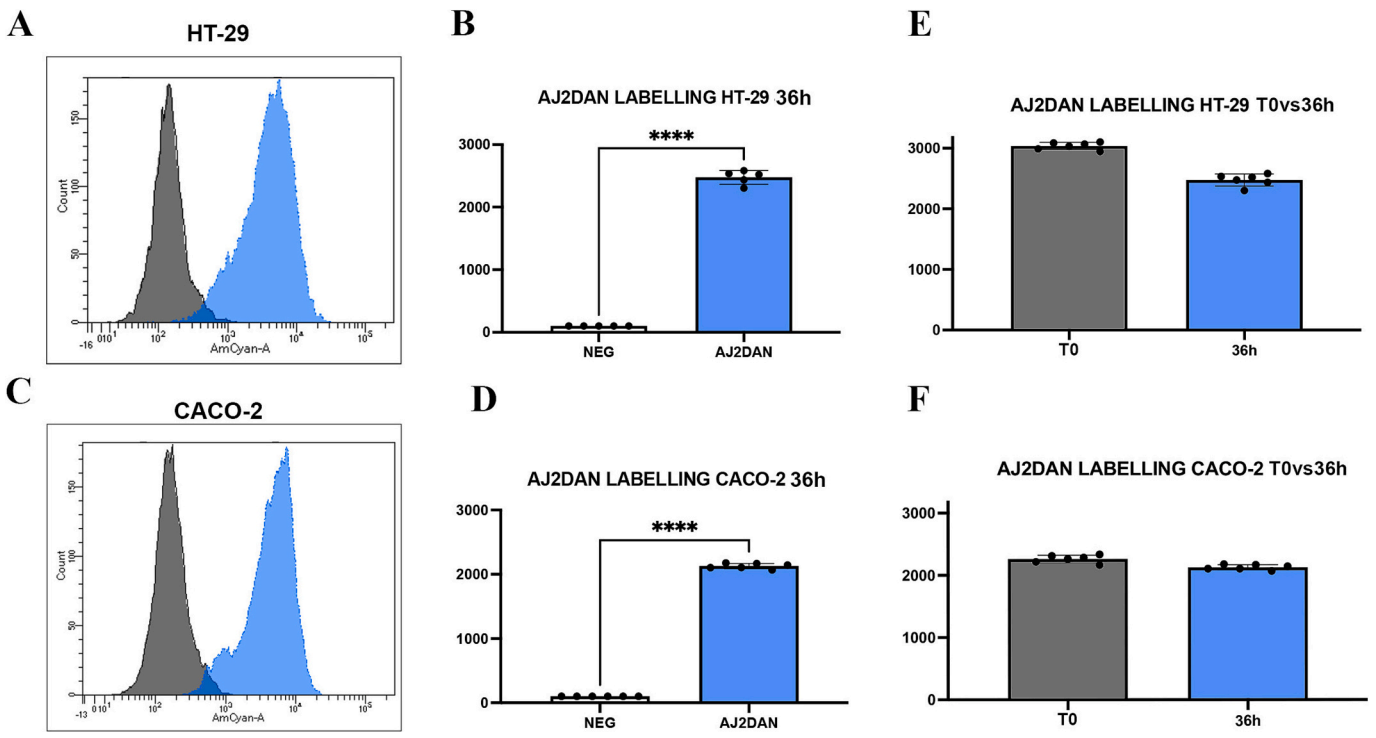

Fig. 9. A HT-29 cells: FC histograms after 36 h from labelling (unlabelled in grey and AJ2DAN-labelled in blue); B Statistical histogram: ratio of MFI from AJ2DAN-labelled and unlabelled HT-29 cells after 36 h from labelling; C Caco-2 cells: FC histograms after 36 h from labelling; D Statistical histogram: ratio of MFI from AJ2DAN-labelled and unlabelled Caco-2 cells after 36 h from labelling. E Statistical histogram: comparison of MFI ratio in HT-29 labelled cells at t0 and 36 h. F Statistical histogram: comparison of MFI ratio in Caco-2 labelled cells at t0 and 36 h. Unpaired *t*-test revealed: **** = $p < 0.0001$. (For interpretation of the references to colour in this figure legend, the reader is referred to the web version of this article.)

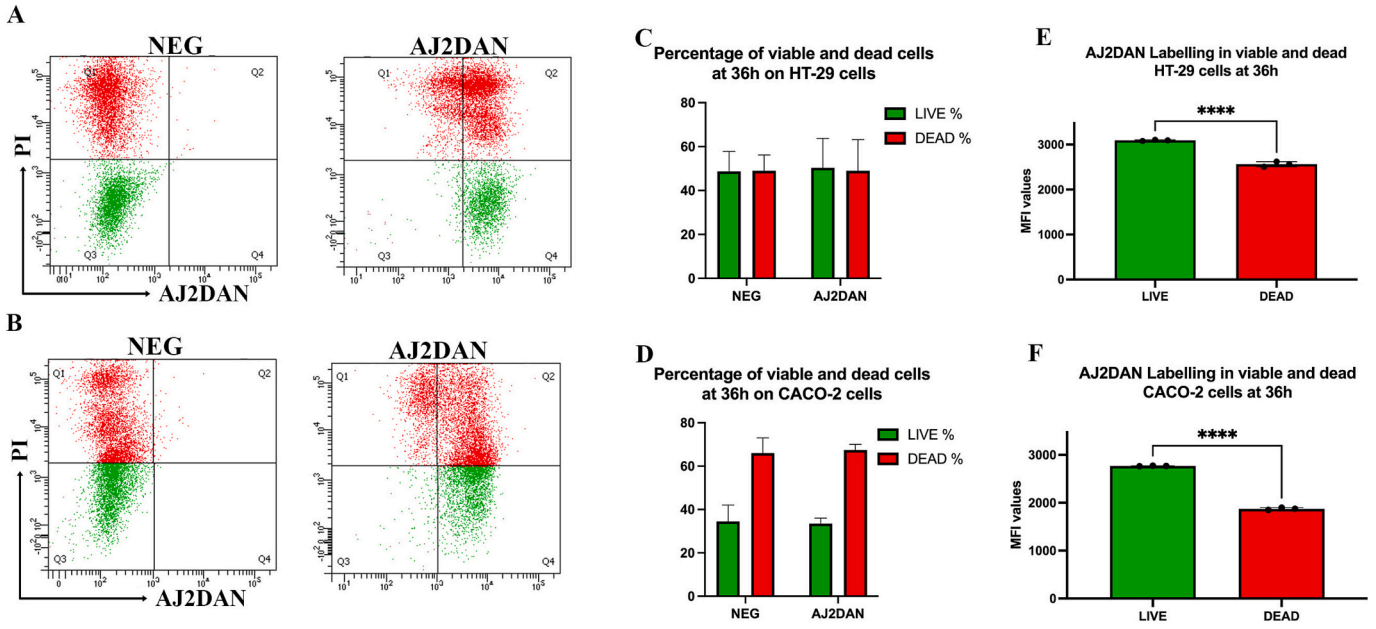

Fig. 10. Dot plot of AJ2DAN *vs* PI in HT-29 cells (A) and in Caco-2 cells (B): unlabelled (left) *vs* AJ2DAN-labelled (right); Percentages of live (green) and dead (red) cells in HT-29 (C) and in Caco-2 (D) after 36 h labelling; Statistical histograms comparison of MFI ratio of AJ2DAN in live and dead cells in HT-29 (E) and in Caco-2 (F). Unpaired *t*-test revealed: **** = $p < 0.0001$. (For interpretation of the references to colour in this figure legend, the reader is referred to the web version of this article.)

been used as an autophagy inhibitor. Indeed, CQ acts at multiple stages of the autophagic process: it inhibits cargo degradation in lysosomes during the final step, while simultaneously accelerating upstream events, such as autophagosome formation, through its inhibitory effect on MTOR (mechanistic target of rapamycin (serine/threonine kinase)). Chloroquine has been demonstrated to inhibit the fusion of autophagosomes with lysosomes [68]. This prevents the lysosomal degradation of autophagosomes, resulting in an increase in the accumulation of

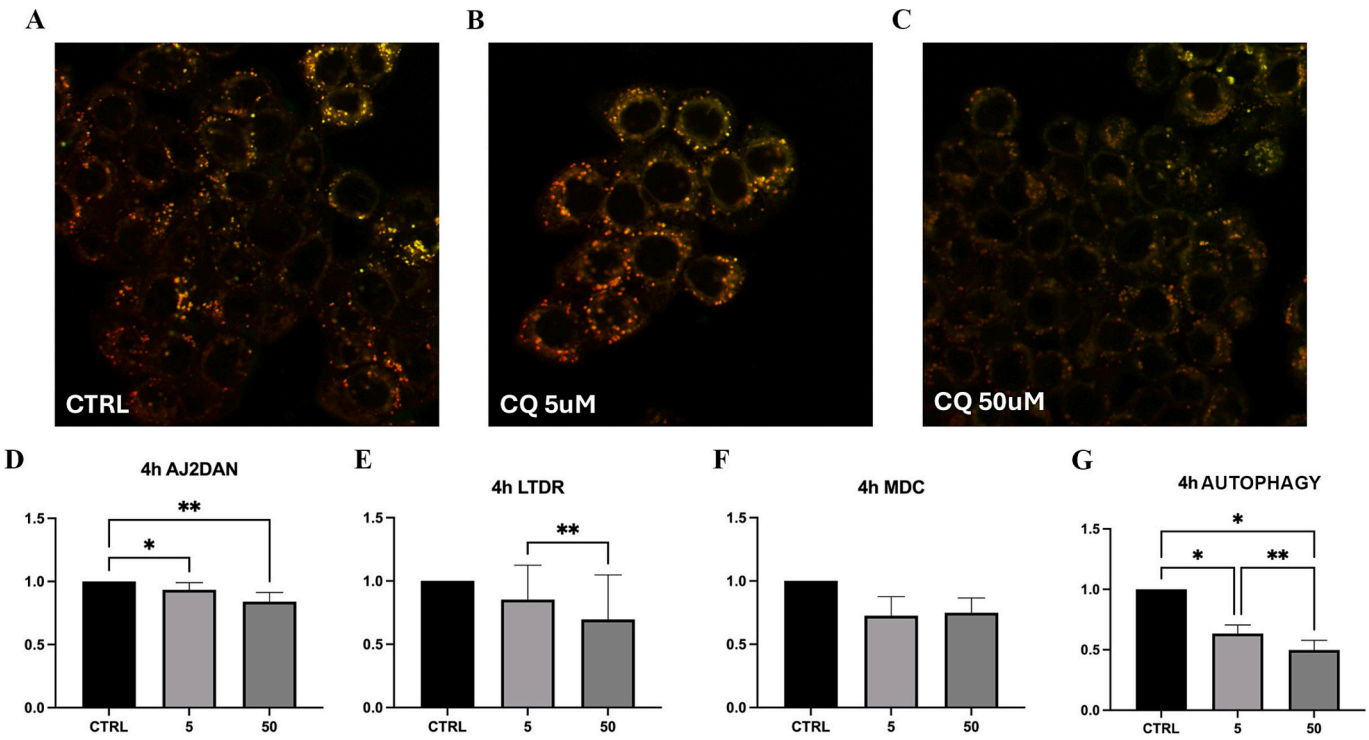

Fig. 11. Single confocal optical sections of: HT-29 CTRL cells at 4 h (A), HT-29 cells treated with 5 μM CQ (B) and 50 μM CQ (C); AJ2DAN (green) and LTDR (red). Statistical histograms of MFI ratio: AJ2DAN (D), LTDR (E), MDC (F), Autophagy kit (G) in CTRL (black), 5 μM (soft grey) and 50 μM (dark grey) CQ-treated cells at 4 h. One-way ANOVA with Bonferroni's multiple comparison revealed: * = $p < 0.05$, ** = $p < 0.01$. (For interpretation of the references to colour in this figure legend, the reader is referred to the web version of this article.)

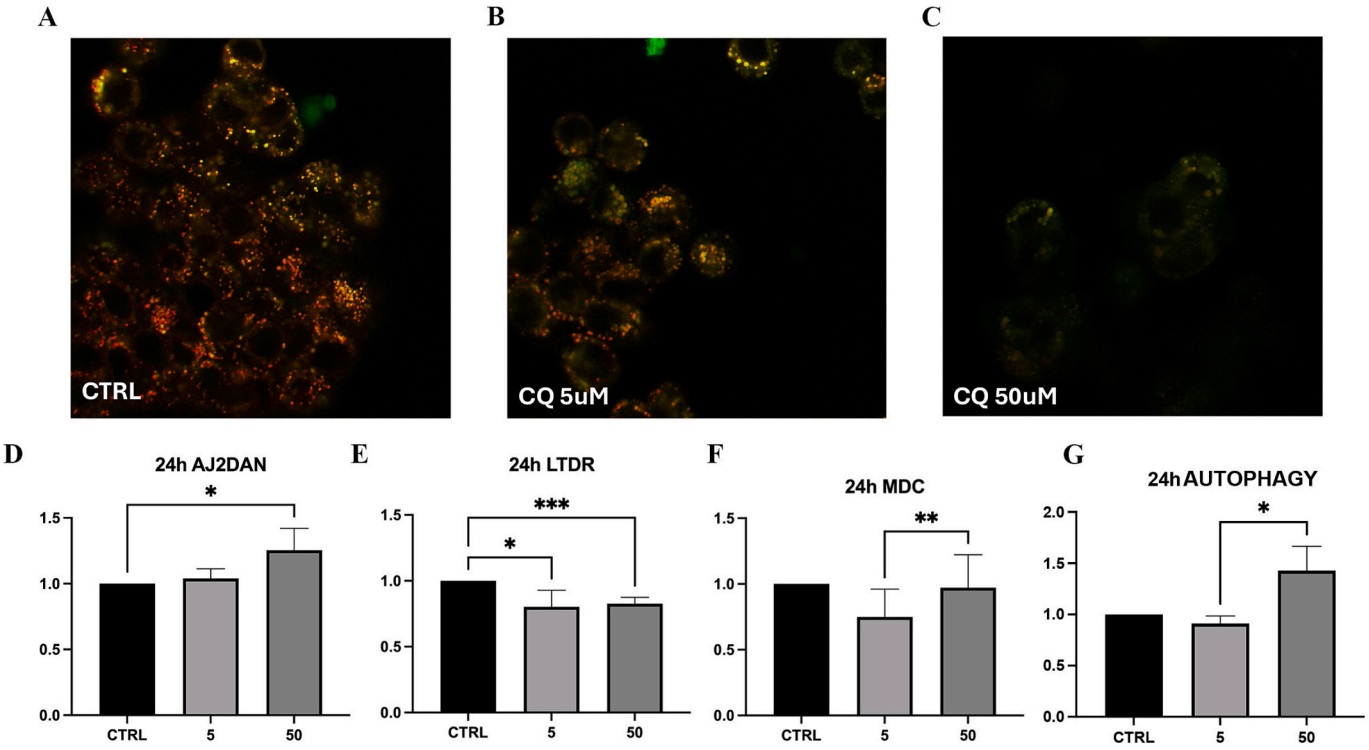

Fig. 12. Single confocal optical sections of: HT-29 CTRL cells at 24 h (A), HT-29 cells treated with 5 μM CQ (B), 50 μM CQ (C); AJ2DAN (green) and LTDR (red). Statistical histograms of MFI ratio: AJ2DAN (D), LTDR (E), MDC (F), Autophagy kit (G) in CTRL (black), 5 μM (soft grey) and 50 μM (dark grey) CQ-treated cells at 24 h.One-way ANOVA with Bonferroni's multiple comparison revealed: * = $p < 0.05$, ** = $p < 0.01$, *** = $p < 0.001$. (For interpretation of the references to colour in this figure legend, the reader is referred to the web version of this article.)

autophagosomes [69]. This is the case of treatment with 5 μM CQ, after 4 h: cells appear enriched of vesicular-like structures, mainly yellow orange (stained by both AJ2DAN and LTDR) but also red (stained only by LTDR). Cardoso and coworkers [70] addressed that initial chloroquine-induced lysosome neutralization was followed by partial recovery of undegraded endocytic, phagocytic and autophagic cargo. Our data propelled us to consider the green vesicular structures (stained by AJ2DAN only) observed after 24 h (Fig. 12B) as undegrading vacuoles, mainly of autophagosome origin. FC quantitative determinations support such consideration well after 4 and 24 h (Fig. 11E *vs* Fig. 12E).

CQ is a lipophilic drug that easily permeates cell membranes and accumulates within lysosomes. Due to its weak basic properties, CQ raises the lysosomal pH from approximately 4 to 6 over a span of several hours. This alteration in the acidic environment leads to the inhibition of lysosomal proteases [71] and, at high concentrations (50 μM), to the disturbance of several cell processes [72]. This evidence is in agreement with our findings, reported in Fig.s 11C and 12C, highlighting HT-29 cells treated by CQ 50 μM for 4 h and 24 h, respectively. In fact, cells display a reduced number of "pale" lysosomes (in other words less functional), whereas they still exhibit well-detectable green vacuolar/vesicular structures (structures that do not fuse with impaired lysosomes), that are the only ones visible after 24 h. FC quantitative data (Fig.s 11D and 12D) confirm and deepen the previous findings, which agree with our preceding studies [41].

On the basis of the findings of Maulucci and coworkers, an increase of AJ2DAN MFI (by FC) or fluorescence puncta (by CM) upon CQ addition can be considered as a raising in the number of autophagic intermediates (amphisomes, formed during autophagy through the fusion between autophagosomes and endosomes), characterized according to autophagic intermediates pH distribution (AIPD) analysis by a continuous pH distribution in the range 4.5–6.5 [73]. This seems to be directly proportional to CQ exposition time and concentration, indeed at CQ 50 μM concentration it is possible to observe the lack of co-localization of "green" AJ2DAN^{positive} vesicles with LTDR^{positive} lysosomes, attesting a specificity for vesicular structures with mild acidic environment (autophagosomes, amphisomes).

Therefore, in the light of FC detection of autophagic vacuoles by both MDC and the Autophagy Kit (Fig.s 11F, G and 12F,G) AJ2DAN can be considered a probe useful for the detection of processes involving autophagic and vesicular trafficking, in cell death and survival studies. It may be useful in characterizing the autophagic process in models for studying anticancer drugs, since suppressors and enhancers of autophagy can control the autophagy-induced cell death [74].

Moreover, the physiological process of endosomal-lysosomal maturation, acidification and sorting systems along the endocytic pathway can incur in abnormalities frequently observed in neurodegenerative diseases, especially Alzheimer's disease (AD). Indeed, a promising therapeutic strategy to suppress atherosclerosis arises from targeting autophagy in major atherogenesis associated cells [75]. For these reasons, the potential efficacy of AJ2DAN labelling on neuronal cell lines of both murine (*e.g.* HT22) and human (*e.g.* SK-N-MC) origin or endothelial cell lines (*e.g.* HUVEC or HMEK) will be taken into account in the future.

Finally, due to its pH dependent fluorescence properties, AJ2DAN may be recommended for cellular labelling both alone and in co-presence of LTDR. Indeed, their combination would help both to finely characterize the tropism of AJ2DAN for intracellular vacuoles/vesicles as well as to detail the maturation steps of the *endo*-lysosomal compartment, involved not only in the autophagic pathway [54] but also in assessing the cellular response to drug delivery systems [76,77]. On the other hand, the pH heterogeneity (5.8–6.2) of autophagosomes is independent from fusion with lysosomes (traced by LTDR), since it derives from differences in the organelle content and membrane protein composition, in the balance of proton pumps and leaks [78] and in the organelles implicated in the origin of the phagophore [79]. All these aspects can modify the labelling properties of AJ2DAN, giving rise to profound modulation of MFI values.

4. Conclusion

In summary, we have developed a new fluorescent molecule, AJ2DAN, by functionalizing the two secondary amine functions of the 1,7-dimethyl-cyclen macrocycle with the dansyl fluorophore. The fluorescent properties of the probe resulted pH-dependent, being AJ2DAN quenched at pH 2 and showing the maximum emission at neutral pH, in agreement with a PCT-based fluorescence mechanism. AJ2DAN proven as a robust probe in aqueous solution, with a large Stokes shift both in water and in several organic solvents.

Tested as a fluorescent probe in biological environment, AJ2DAN exhibited a long-retained fluorescence in both HT-29 and Caco-2 tested cell lines, moreover it resulted not toxic for the cells, allowing its use in panels to study cell death induction. Furthermore, since Chloroquine inhibits autophagic flux by decreasing autophagosome-lysosome fusion, this drug was taken into account in the designed working plan. The observed increase of AJ2DAN MFI (by FC) or fluorescence puncta (by CM) upon Chloroquine addition may be related with a higher number of autophagic intermediates, characterized according to autophagic intermediates pH distribution (AIPD) analysis by a continuous pH distribution in the range 4.5–6.5.

Nevertheless, the pH behaviour is only secondary compared to the ability of AJ2DAN to inform about the quantity (FC) and distribution (CM) of a very dynamic *endo*-lysosomal compartment, that is also maturely linked to pH variations.

All the findings point at considering AJ2DAN as a useful probe for the detection of processes involving autophagic and vesicular trafficking, in cell death and survival studies through flow cytometric analysis. AJ2DAN may be recommended for both labelling and co-labeling with LTDR, to finely characterize the tropism of AJ2DAN for intracellular vacuoles/vesicles as well as to detail the maturation steps of the endo-lysosomal compartment.

Finally, compared to the previously studied compound AJ2NBD, the new probe AJ2DAN may represent an evolutionary step, due to *i)* the more favorable excitation and emission spectra (better combination with other fluorochromes in multicolor analyses) and *ii)* the significant decrease in the number and/or functions of vesicular-like AJ2DAN-labelled structures in the PI^{positive} dying cells, that can represent an additional useful information in cell-death inducing studies.

Declaration of competing interest

The authors declare that they do not have known competing financial interests or personal relationships that could have appeared to influence the work reported in this paper.

Acknowledgments

We gratefully acknowledge Dr. Gianluca Ambrosi for his help with NMR measurements, Dr. Federica Biancucci for HRMS analysis and Dr. Ludovica Di Fabrizio for her laboratory assistance. This work has been funded by the European Union - NextGenerationEU, Mission 4, Component 1, under the Italian Ministry of University and Research (MUR) National Innovation Ecosystem grant ECS00000041 - VITALITY - CUP H33C22000430006.

Appendix A. Supplementary data

Supplementary data to this article can be found online at https://doi.org/10.1016/j.ica.2025.122620.

Data availability

Data will be made available on request.

References

[1] G.E. Giacomazzo, D. Paderni, L. Giorgi, M. Formica, L. Mari, R. Montis, L. Conti, E. Macedi, B. Valtancoli, C. Giorgi, V. Fusi, A new family of macrocyclic Polyamino Biphenolic ligands: Acid-Base study, Zn(II) coordination and glyphosate/AMPA binding, Molecules 28 (2023) 2031, https://doi.org/10.3390/molecules28052031.

[2] E. Macedi, L. Giorgi, M. Formica, P. Rossi, D. Paderni, P. Paoli, V. Fusi, A Tetranuclear copper(II)/calcium(II) complex as dual Chemosensor for colorimetric and fluorescent detection of non-steroidal anti-inflammatory drugs, Chempluschem 88 (2023) e202200364, https://doi.org/10.1002/cplu.202200364.

[3] D. Paderni, E. Macedi, L. Lvova, G. Ambrosi, M. Formica, L. Giorgi, R. Paolesse, V. Fusi, Selective detection of Mg2+ for sensing applications in drinking water, Chem. - A Eur. J. 28 (2022), https://doi.org/10.1002/chem.202201062.

[4] E.R.H. Walter, C. Hogg, D. Parker, J.A. Gareth Williams, Designing magnesium-selective ligands using coordination chemistry principles, Coord. Chem. Rev. 428 (2021) 213622, https://doi.org/10.1016/J.CCR.2020.213622.

[5] T.S. Lazarou, D. Buccella, Advances in imaging of understudied ions in signaling: a focus on magnesium, Curr. Opin. Chem. Biol. 57 (2020) 27–33, https://doi.org/10.1016/J.CBPA.2020.04.002.

[6] P.S. Hariharan, S.P. Anthony, Selective fluorescence sensing of Mg2+ions by Schiff base chemosensor: effect of diamine structural rigidity and solvent, RSC Adv. 40 (2014) 41565–41571, https://doi.org/10.1039/c4ra05827e.

[7] M. Liu, X. Yu, M. Li, N. Liao, A. Bi, Y. Jiang, S. Liu, Z. Gong, W. Zeng, Fluorescent probes for the detection of magnesium ions (Mg2+): from design to application, RSC Adv. 8 (2018) 12573–12587, https://doi.org/10.1039/C8RA00946E.

[8] G. Ambrosi, M. Micheloni, D. Paderni, M. Formica, L. Giorgi, V. Fusi, Fluorescent macrocyclic chemosensor for Zn(II) detection at alkaline pH values, Supramol. Chem. 32 (2020) 139–149, https://doi.org/10.1080/10610278.2020.1713324.

[9] G. Ambrosi, M. Formica, V. Fusi, L. Giorgi, E. Macedi, M. Micheloni, G. Piersanti, R. Pontellini, New family of polyamine macrocycles containing 2,5-diphenyl[1,3,4] oxadiazole as a signaling unit. Synthesis, acid-base and spectrophotometric properties, Org. Biomol. Chem. 8 (2010) 1471–1478, https://doi.org/10.1039/b921053a.

[10] D. Paderni, L. Giorgi, M. Voccia, M. Formica, L. Caporaso, E. Macedi, V. Fusi, A new Benzoxazole-based fluorescent macrocyclic Chemosensor for optical detection of Zn2+ and Cd2+, Chemosensors 10 (2022) 188, https://doi.org/10.3390/CHEMOSENSORS10050188/S1.

[11] S. Amatori, G. Ambrosi, M. Fanelli, M. Formica, V. Fusi, L. Giorgi, E. Macedi, M. Micheloni, P. Paoli, R. Pontellini, P. Rossi, M.A. Varrese, Multi-use NBD-based tetra-amino macrocycle: fluorescent probe for metals and anions and live cell marker, Chem. - A Eur. J. 18 (2012) 4274–4284, https://doi.org/10.1002/chem.201103135.

[12] G. Ambrosi, M. Formica, V. Fusi, L. Giorgi, E. Macedi, G. Piersanti, M. Retini, M. A. Varrese, G. Zappia, New coumarin-urea based receptor for anions: a selective off-on fluorescence response to fluoride, Tetrahedron 68 (2012) 3768–3775, https://doi.org/10.1016/J.TET.2012.02.067.

[13] D. Paderni, G. Barone, L. Giorgi, M. Formica, E. Macedi, V. Fusi, A novel 2,6-bis (benzoxazolyl)phenol macrocyclic chemosensor with enhanced fluorophore properties by photoinduced intramolecular proton transfer, Dalton Trans. (2023) 3716–3724, https://doi.org/10.1039/d3dt00140g.

[14] X. Han, Y. Wang, Y. Huang, X. Wang, J. Choo, L. Chen, Fluorescent probes for biomolecule detection under environmental stress, J. Hazard. Mater. 431 (2022), https://doi.org/10.1016/j.jhazmat.2022.128527.

[15] W.T. Dou, H.H. Han, A.C. Sedgwick, G.B. Zhu, Y. Zang, X.R. Yang, J. Yoon, T. D. James, J. Li, X.P. He, Fluorescent probes for the detection of disease-associated biomarkers, Sci. Bull. 67 (2022) 853–878, https://doi.org/10.1016/J.SCIB.2022.01.014.

[16] G. Picci, M.C. Aragoni, M. Arca, C. Caltagirone, M. Formica, V. Fusi, L. Giorgi, F. Ingargiola, V. Lippolis, E. Macedi, L. Mancini, L. Mummolo, L. Prodi, Fluorescent sensing of non-steroidal anti-inflammatory drugs naproxen and ketoprofen by dansylated squaramide-based receptors, Org. Biomol. Chem. 21 (2023) 2968–2975, https://doi.org/10.1039/d3ob00324h.

[17] W. Xu, Z. Zeng, J.H. Jiang, Y.T. Chang, L. Yuan, Discerning the chemistry in individual organelles with small-molecule fluorescent probes, Angew. Chem. Int. Ed. 55 (2016) 13658–13699, https://doi.org/10.1002/ANIE.201510721.

[18] L. Wu, J. Huang, K. Pu, T.D. James, Dual-locked spectroscopic probes for sensing and therapy, Nat. Rev. Chem. 5 (2021) (2021) 406–421, https://doi.org/10.1038/s41570-021-00277-2, 56.

[19] J. Yin, L. Huang, L. Wu, J. Li, T.D. James, W. Lin, Small molecule based fluorescent chemosensors for imaging the microenvironment within specific cellular regions, Chem. Soc. Rev. 50 (2021) 12098–12150, https://doi.org/10.1039/D1CS00645B.

[20] X. Huang, J. Song, B.C. Yung, X. Huang, Y. Xiong, X. Chen, Ratiometric optical nanoprobes enable accurate molecular detection and imaging, Chem. Soc. Rev. 47 (2018) 2873–2920, https://doi.org/10.1039/C7CS00612H.

[21] Z. Hu, C. Fang, B. Li, Z. Zhang, C. Cao, M. Cai, S. Su, X. Sun, X. Shi, C. Li, T. Zhou, Y. Zhang, C. Chi, P. He, X. Xia, Y. Chen, S.S. Gambhir, Z. Cheng, J. Tian, First-in-human liver-tumour surgery guided by multispectral fluorescence imaging in the visible and near-infrared-I/II windows, Nat. Biomed. Eng. 4 (2019) (2019) 259–271, https://doi.org/10.1038/s41551-019-0494-0, 43.

[22] X. Zhao, J. Liu, J. Fan, H. Chao, X. Peng, Recent progress in photosensitizers for overcoming the challenges of photodynamic therapy: from molecular design to application, Chem. Soc. Rev. 50 (2021) 4185–4219, https://doi.org/10.1039/D0CS00173B.

[23] L. Conti, E. Macedi, C. Giorgi, B. Valtancoli, V. Fusi, Combination of light and Ru (II) polypyridyl complexes: recent advances in the development of new anticancer drugs, Coord. Chem. Rev. 469 (2022) 214656, https://doi.org/10.1016/j.ccr.2022.214656.

[24] V. Vingtdeux, M. Hamdane, S. Bégard, A. Loyens, A. Delacourte, J.C. Beauvillain, L. Buée, P. Marambaud, N. Sergeant, Intracellular pH regulates amyloid precursor protein intracellular domain accumulation, Neurobiol. Dis. 25 (2007) 686–696, https://doi.org/10.1016/J.NBD.2006.09.019.

[25] H.J. Kim, C.H. Heo, H.M. Kim, Benzimidazole-based ratiometric two-photon fluorescent probes for acidic pH in live cells and tissues, J. Am. Chem. Soc. 135 (2013) 17969–17977, https://doi.org/10.1021/JA409971K.

[26] R. Li, X. Chai, X. Cui, Y. Jiang, D. Zhang, T. Wang, A fluorescence resonance energy transfer based pH probe for visualizing acidification in fungal cells, Sensors Actuators B Chem. 274 (2018) 533–540, https://doi.org/10.1016/J.SNB.2018.07.134.

[27] Q. Zhu, Z. Li, L. Mu, X. Zeng, C. Redshaw, G. Wei, A quinoline-based fluorometric and colorimetric dual-modal pH probe and its application in bioimaging, Spectrochim, Acta Part A Mol. Biomol. Spectrosc. 188 (2018) 230–236, https://doi.org/10.1016/J.SAA.2017.06.071.

[28] Y. Wang, L. Zeng, J. Zhou, B. Jiang, L. Zhao, C. Wang, B. Xu, A dansyl fluorescent pH probe with wide responsive range in aqueous solution, Spectrochim, Acta Part A Mol. Biomol. Spectrosc. 223 (2019) 117348, https://doi.org/10.1016/J.SAA.2019.117348.

[29] Y. Liu, Y. Wang, L. Zhao, B. Xu, Development of a simple Dansyl-based PH fluorescent probe in acidic medium and its application in cell imaging, J. Fluoresc. 32 (2022) 227–233, https://doi.org/10.1007/S10895-021-02843-9.

[30] A.V. Saura, M.J. Marín, M.I. Burguete, D.A. Russell, F. Galindo, S.V. Luis, The synthesis of new fluorescent bichromophoric compounds as ratiometric pH probes for intracellular measurements, Org. Biomol. Chem. 13 (2015) 7736–7749, https://doi.org/10.1039/C5OB00704F.

[31] Y. Zhang, J. Cao, L. Ding, Fluorescent ensemble based on dansyl derivative/SDS assemblies as selective sensor for asp and Glu in aqueous solution, J. Photochem. Photobiol. A Chem. 333 (2017) 56–62, https://doi.org/10.1016/J.JPHOTOCHEM.2016.10.018.

[32] C. Sha, Y. Chen, Y. Chen, D. Xu, An easily prepared fluorescent pH probe based on Dansyl, J. Fluoresc. 26 (2016) 1709–1714, https://doi.org/10.1007/S10895-016-1861-9.

[33] M. Zhang, S. Zheng, L. Ma, M. Zhao, L. Deng, L. Yang, L.J. Ma, Dansyl-8-aminoquinoline as a sensitive pH fluorescent probe with dual-responsive ranges in aqueous solutions, Spectrochim, Acta Part A Mol. Biomol. Spectrosc. 124 (2014) 682–686, https://doi.org/10.1016/J.SAA.2013.12.062.

[34] G. Bergamaschi, A. Miljkovic, S. Marcheggiani, A. Poggi, Synthesis and study in solution of a new Dansyl-modified Azacryptand, Int. J. Inorg. Chem. 2016 (2016) 3415690, https://doi.org/10.1155/2016/3415690.

[35] X. Zuo-An, Z. Dan, Y. Xiao, Synthesis and fluorescent properties of a novel Dansyl-based fluorescent probe for Hg2+, J. Chem. Res. 38 (2014) 108–110, https://doi.org/10.3184/174751914X13895467018450.

[36] J. Sanmartín-Matalobos, P. Bermejo-Barrera, Y. Alves-Iglesias, A.M. García-Deibe, M. Fondo, Synthesis and characterization of a Dansyl-based fluorescent probe for analytical purposes, Chem. Process. 8 (2022) 76, https://doi.org/10.3390/ECSOC-25-11775.

[37] I. Pereira-Gomes, F. Duarte, G.M. Dobrikov, I. Slavchev, A. Kurutos, J.L. Capelo-Martinez, H.M. Santos, C. Lodeiro, Tetra dansylamides substituted cyclen and cyclam macrocycles as fluorescent sensing probes for metal ions and temperature-responsive materials in dopped polymers, Dyes Pigments 232 (2025) 112461, https://doi.org/10.1016/J.DYEPIG.2024.112461.

[38] S.A. Sander, J.R. Morrow, Zn(II) complexes that trigger a DNA conformational switch 452, 2016, pp. 90–97.

[39] L.L. O'Neil, O. Wiest, Sequence dependence in base flipping : experimental and computational studies, Org. Biomol. Chem. 6 (2008) 485–492, https://doi.org/10.1039/b713318a.

[40] J.Y. Kim, S. Sarkar, K.N. Bobba, P.T. Huynh, A. Bhise, J. Yoo, Development of dansyl based copper(II) complex to detect hydrogen sulfide in hypoxia, Org. Biomol. Chem. 17 (2019) 7088–7094, https://doi.org/10.1039/c9ob00948e.

[41] B. Canonico, L. Giorgi, M.G. Nasoni, M. Montanari, G. Ambrosi, M. Formica, C. Ciacci, P. Ambrogini, S. Papa, V. Fusi, F. Luchetti, Synthesis and biological characterization of a new fluorescent probe for vesicular trafficking based on polyazamacrocycle derivative, Biol. Chem. 402 (2021) 1225–1237, https://doi.org/10.1515/HSZ-2021-0204.

[42] V. Fusi, M. Formica, L. Giorgi, S. Papa, F. Lucchetti, B. Canonico, WO2019077527 - heterocyclic Compounds as Fluorescent Probes for Detection in Biological Systems, wo/2019/077527. https://patentscope.wipo.int/search/en/detail.jsf?docId=WO2019077527, 2019.

[43] W. Koch, M.C. Holthausen, A Chemist's Guide to Density Functional Theory, 2nd Ed, Wiley-VCH Verlag GmbH, 2001.

[44] G. Piersanti, M.A. Varrese, V. Fusi, L. Giorgi, G. Zappia, Short and straightforward synthesis of 1,7-dimethyl-1,4,7,10-tetraazacyclododecane, Tetrahedron Lett. 51 (2010) 3436–3438, https://doi.org/10.1016/J.TETLET.2010.04.115.

[45] J.P. Perdew, Density-functional approximation for the correlation energy of the inhomogeneous electron gas, Erratum Phys. Rev. B 34 (1986) 7406, https://doi.org/10.1103/PhysRevB.34.7406. Phys. Rev. B. 33 (1986) 8822. doi:10.1103/PhysRevB.33.8822.

[46] J.P. Perdew, Erratum: density-functional approximation for the correlation energy of the inhomogeneous electron gas, Phys. Rev. B 34 (1986) 7406, https://doi.org/10.1103/PhysRevB.34.7406.

[47] A.D. Becke, Density-functional exchange-energy approximation with correct asymptotic behavior, Phys. Rev. A 38 (1988) 3098, https://doi.org/10.1103/PhysRevA.38.3098.

[48] M.J. Frisch, G.W. Trucks, H.B. Schlegel, G.E. Scuseria, M.A. Robb, J.R. Cheeseman, G. Scalmani, V. Barone, G.A. Petersson, H. Nakatsuji, X. Li, M. Caricato, A. V. Marenich, J. Bloino, B.G. Janesko, R. Gomperts, B. Mennucci, H.P. Hratchian, J. V. Ortiz, A.F. Izmaylov, J.L. Sonnenberg, D. Williams-Young, F. Ding, F. Lipparini, F. Egidi, J. Goings, B. Peng, A. Petrone, T. Henderson, D. Ranasinghe, V. G. Zakrzewski, J. Gao, N. Rega, G. Zheng, W. Liang, M. Hada, M. Ehara, K. Toyota, R. Fukuda, J. Hasegawa, M. Ishida, T. Nakajima, Y. Honda, O. Kitao, H. Nakai, T. Vreven, K. Throssell, J.J.A. Montgomery, J.E. Peralta, F. Ogliaro, M.J. Bearpark, J.J. Heyd, E.N. Brothers, K.N. Kudin, V.N. Staroverov, T.A. Keith, R. Kobayashi, J. Normand, K. Raghavachari, A.P. Rendell, J.C. Burant, S.S. Iyengar, J. Tomasi, M. Cossi, J.M. Millam, M. Klene, C. Adamo, R. Cammi, J.W. Ochterski, R.L. Martin, K. Morokuma, O. Farkas, J.B. Foresman, D.J. Fox, Gaussian 16, Revision C.01, Gaussian Inc., Wallingford CT, 2019.
[49] A. Schäfer, H. Horn, R. Ahlrichs, Fully optimized contracted Gaussian basis sets for atoms Li to Kr, J. Chem. Phys. 97 (1992) 2571–2577, https://doi.org/10.1063/1.463096.
[50] T.H. Dunning Jr., P.J. Hay, Modern Theoretical Chemsitry vol. 3, Plenum, New York, 1977.
[51] S. Grimme, S. Ehrlich, L. Goerigk, Effect of the damping function in dispersion corrected density functional theory, J. Comput. Chem. 32 (2011) 1456–1465.
[52] B. Canonico, M. Cangiotti, M. Montanari, S. Papa, V. Fusi, L. Giorgi, C. Ciacci, M. F. Ottaviani, D. Staneva, I. Grabchev, Characterization of a fluorescent 1,8-naphthalimide-functionalized PAMAM dendrimer and its cu(ii) complexes as cytotoxic drugs: EPR and biological studies in myeloid tumor cells, Biol. Chem. 403 (2022) 345–360, https://doi.org/10.1515/HSZ-2021-0388.
[53] G.Y. Shen, J.H. Shin, Y.S. Song, H.W. Joo, I.H. Park, J.H. Seong, N.K. Shin, A. H. Lee, Y.J. Cho, Y. Lee, Y.H. Lim, H. Kim, K.S. Kim, Role of autophagy in granulocyte-colony stimulating factor induced anti-apoptotic effects in diabetic cardiomyopathy, Diabetes Metab. J. 45 (2021) 594–605, https://doi.org/10.4093/DMJ.2020.0049.
[54] D.J. Klionsky, et al., Guidelines for the use and interpretation of assays for monitoring autophagy (4th edition)1, Autophagy 17 (2021) 1–382, https://doi.org/10.1080/15548627.2020.1797280.
[55] S. Aoki, Y. Tomiyama, Y. Kageyama, Y. Yamada, M. Shiro, E. Kimura, Photolysis of the sulfonamide bond of metal complexes of N-Dansyl-1,4,7,10-tetraazacyclododecane in aqueous solution: A mechanistic study and application to the photorepair of cis,syn-cyclobutane thymine photodimer, Chem. – An Asian J. 4 (2009) 561–573, https://doi.org/10.1002/ASIA.200800428.
[56] Y. Zheng, A. Hashidzume, A. Harada, pH-responsive self-assembly by molecular recognition on a macroscopic scale, Macromol. Rapid Commun. 34 (2013) 1062–1066, https://doi.org/10.1002/MARC.201300324.
[57] T. Koike, T. Watanabe, S. Aoki, E. Kimura, M. Shiro, A novel biomimetic zinc(II)-fluorophore, dansylamidoethyl-pendant macrocyclic Tetraamine 1,4,7,10-Tetraazacyclododecane (Cyclen), J. Am. Chem. Soc. 118 (1996) 12696–12703, https://doi.org/10.1021/ja962527a.
[58] X. Qu, D.A.R.S. Latino, J. Aires-de-Sousa, A big data approach to the ultra-fast prediction of DFT-calculated bond energies, J. Chemother. 5 (2013) 1–13, https://doi.org/10.1186/1758-2946-5-34.
[59] P.C. St, Y. John, Y. Guan, S. Kim, R.S. Paton Kim, Prediction of organic homolytic bond dissociation enthalpies at near chemical accuracy with sub-second computational cost, Nat. Commun. 11 (2020) 1–12, https://doi.org/10.1038/s41467-020-16201-z.
[60] H. Bhakhoa, L. Rhyman, E.P. Lee, D.K.W. Mok, P. Ramasami, J.M. Dyke, A study of the group 1 metal tetra-aza macrocyclic complexes [M(Me4cyclen)(L)]+ using electronic structure calculations, Dalton Trans. 46 (2017) 15301–15310, https://doi.org/10.1039/c7dt03002a.
[61] D. Paderni, M. Voccia, E. Macedi, M. Formica, L. Giorgi, L. Caporaso, V. Fusi, A combined solid state, solution and DFT study of a dimethyl- cyclen-Pd(II) complex, Dalton Trans. 53 (2024) 14300–14314, https://doi.org/10.1039/D4DT01791A.
[62] E. Gheytanchi, M. Naseri, F. Karimi-Busheri, F. Atyabi, E.S. Mirsharif, M. Bozorgmehr, R. Ghods, Z. Madjd, Morphological and molecular characteristics of spheroid formation in HT-29 and Caco-2 colorectal cancer cell lines, Cancer Cell Int. 21 (2021) 1–16, https://doi.org/10.1186/S12935-021-01898-9/FIGURES/4.
[63] R.L. Siegel, K.D. Miller, A. Jemal, Cancer statistics, 2020, CA, Cancer J. Clin. 70 (2020) 7–30, https://doi.org/10.3322/CAAC.21590.
[64] C. Karthika, R. Sureshkumar, M. Zehravi, R. Akter, F. Ali, S. Ramproshad, B. Mondal, M.K. Kundu, A. Dey, M.H. Rahman, A. Antonescu, S. Cavalu, Multidrug resistance in cancer cells: Focus on a possible strategy plan to address colon carcinoma cells, Life 12 (2022) 811, https://doi.org/10.3390/LIFE12060811.
[65] N.A. Hussein, S. Malla, M.A. Pasternak, D. Terrero, N.G. Brown, C.R. Ashby, Y. G. Assaraf, Z.S. Chen, A.K. Tiwari, The role of endolysosomal trafficking in anticancer drug resistance, Drug Resist. Updat. 57 (2021) 100769, https://doi.org/10.1016/J.DRUP.2021.100769.
[66] L. Hunt, D.L. Hacker, F. Grosjean, M. De Jesus, L. Uebersax, M. Jordan, F.M. Wurm, Low-temperature pausing of cultivated mammalian cells, Biotechnol. Bioeng. 89 (2005) 157–163, https://doi.org/10.1002/BIT.20320.
[67] V.R. Solomon, H. Lee, Chloroquine and its analogs: a new promise of an old drug for effective and safe cancer therapies, Eur. J. Pharmacol. 625 (2009) 220–233, https://doi.org/10.1016/J.EJPHAR.2009.06.063.
[68] M. Mauthe, I. Orhon, C. Rocchi, X. Zhou, M. Luhr, K.J. Hijlkema, R.P. Coppes, N. Engedal, M. Mari, F. Reggiori, Chloroquine inhibits autophagic flux by decreasing autophagosome-lysosome fusion, Autophagy 14 (2018) 1435–1455, https://doi.org/10.1080/15548627.2018.1474314.
[69] Y. Ishibashi, O. Nakamura, Y. Yamagami, H. Nishimura, N. Fukuoka, T. Yamamoto, Chloroquine enhances rapamycin-induced apoptosis in MG63 cells, Anticancer Res. 39 (2019) 649–654, https://doi.org/10.21873/ANTICANRES.13159.
[70] M.H. Cardoso, M.J. Hall, T. Burgoyne, P. Fale, T. Storm, C. Escrevente, P. Antas, M. C. Seabra, C.E. Futter, Impaired lysosome reformation in chloroquine-treated retinal pigment epithelial cells, Invest. Ophthalmol. Vis. Sci. 64 (2023) 10, https://doi.org/10.1167/IOVS.64.11.10.
[71] T. Zhang, F. Huo, W. Zhang, J. Chao, C. Yin, Ultra-pH-sensitive sensor for visualization of lysosomal autophagy, drug-induced pH alteration and malignant tumors microenvironment, Sensors Actuators B Chem. 345 (2021) 130393, https://doi.org/10.1016/J.SNB.2021.130393.
[72] I.R. Rao, A. Kolakemar, S.V. Shenoy, R.A. Prabhu, S.P. Nagaraju, D. Rangaswamy, M.V. Bhojaraja, Hydroxychloroquine in nephrology: current status and future directions, J. Nephrol. 36 (2023) 2191–2208, https://doi.org/10.1007/S40620-023-01733-6.
[73] G. Maulucci, M. Chiarpotto, M. Papi, D. Samengo, G. Pani, M. De Spirito, Quantitative analysis of autophagic flux by confocal pH-imaging of autophagic intermediates, Autophagy 11 (2015) 1905–1916, https://doi.org/10.1080/15548627.2015.1084455.
[74] Y. Chen, S.B. Gibson, Three dimensions of autophagy in regulating tumor growth: cell survival/death, cell proliferation, and tumor dormancy, Biochim. Biophys. Acta Mol. basis Dis. 1867 (2021) 166265, https://doi.org/10.1016/J.BBADIS.2021.166265.
[75] S. Wang, R. Yuan, M. Liu, Y. Zhang, B. Jia, J. Ruan, J. Shen, Y. Zhang, M. Liu, T. Wang, Targeting autophagy in atherosclerosis: advances and therapeutic potential of natural bioactive compounds from herbal medicines and natural products, Biomed. Pharmacother. 155 (2022) 113712, https://doi.org/10.1016/J.BIOPHA.2022.113712.
[76] S. Tavakol, M. Ashrafizadeh, S. Deng, M. Azarian, A. Abdoli, M. Motavaf, D. Poormoghadam, H. Khanbabaei, E. Ghasemipour Afshar, A. Mandegary, A. Pardakhty, C.T. Yap, R. Mohammadinejad, A. Prem Kumar, Autophagy modulators: mechanistic aspects and drug delivery systems, Biomolecules 9 (2019) 530, https://doi.org/10.3390/BIOM9100530.
[77] B. Canonico, S. Pricl, S. Biagiotti, M. Guescini, C. Barattini, M. Montanari, G. Panza, D. Lopez, S. Papa, D.J. Klionsky, New-generation drug delivery systems (DDSs) in Anticancer Strategies: Impact of Autophagy and its Modulation, in: Interdiscipline Cancer Results, Springer, Cham, 2024, pp. 1–49, https://doi.org/10.1007/16833_2024_397.
[78] P. Paroutis, N. Touret, S. Grinstein, The pH of the secretory pathway: measurement, determinants, and regulation, Physiology 19 (2004) 207–215, https://doi.org/10.1152/PHYSIOL.00005.2004/ASSET/IMAGES/LARGE/Y-0005-4-06.JPEG.
[79] S.A. Tooze, T. Yoshimori, The origin of the autophagosomal membrane, Nat. Cell Biol. 12 (2010) (2010) 831–835, https://doi.org/10.1038/ncb0910-831, 129.